A Comparison of the Ka-Band Deep-Space Link with the X-Band Link through Emulation

Shervin Shambayati*

In this article the performance of the 32-GHz (Ka-band) deep-space link is compared to that of the 8.41-GHz (X-band) link through emulation. Sky brightness time series from water vapor radiometers (WVRs) and advanced WVRs (AWVRs) were used to emulate the effects of increased system noise temperature (SNT) and line-of-sight atmospheric attenuation due for both X-band and Ka-band. Models for Deep Space Network (DSN) ground antennas were used to obtain ground antenna gain and system noise temperature performance. Mars Reconnaissance Orbiter (MRO) X-band and Ka-band capabilities with slightly different coding and data rates were chosen for the spacecraft link design and emulation. A total of 207 passes (69 per DSN complex) from MRO's DSN tracking schedule were selected for these emulations. For each pass, the actual link geometry was used to design and emulate the link. The Ka-band link was designed so that the expected pass capacity is maximized with at most two data rates, subject to a minimum availability requirement (MAR). Two X-band link designs were used. The first design approach, similar to Ka-band, maximized the expected link capacity with at most two data rates subject to a MAR. The second design approach was similar to the current MRO link design practice. In this approach, the X-band link was designed for operations above 20 deg elevation with a single data rate that has at least 1 dB of margin over 90 percent supportable data rate at 20 deg elevation. The analysis provides continuity and completeness statistics as well as delay-throughput performance characteristics for both Ka-band and X-band. The analysis indicates that the optimized X-band link has only a 2-dB advantage over current practice in terms of capacity and the Ka-band link offers an approximately 5.5-dB advantage over current practice (normalized for onboard DC power used). The analysis also indicates that even with a 99 percent MAR, the Ka-band link suffers an order of magnitude more losses than the current X-band practice. Therefore, it is recommended that the Ka-band link be designed for maximum expected capacity and additional onboard storage and retransmission schemes be used to assure data completeness, provided that the delay requirements on the data are not too stringent. The

---

*Communication Architectures and Research Section.

The research described in this publication was performed at the Jet Propulsion Laboratory, California Institute of Technology, under a contract with the National Aeronautics and Space Administration.

results also show that a Ka-band link designed with 80 percent MAR offers near-maximum capacity with significantly smaller losses than lower MAR values. Therefore, it is recommended that 80 percent MAR be used for future Ka-band link designs. The delay-throughput performance results indicate that a spacecraft storage equal to three to four times the maximum amount of new data collected before a pass is sufficient to assure nearly 100 percent data completeness. This result, however, needs to be verified through a more systematic analysis.

I. Introduction

Early analysis of deep-space 32-GHz (Ka-band) frequency had indicated that in order to maximize the data return on the Ka-band link, the link has to be operated with about 80 percent to 90 percent weather availability, depending on the elevation and the site [1]. The implications of this are that if a data completeness of greater than 90 percent on the data is desired, some sort of retransmission scheme needs to be employed. This in turn implies that the spacecraft needs to have excess storage to store the data and excess capacity on the link for retransmissions. A preliminary analysis was performed [2] to evaluate the required channel capacity and buffer size as a function of data collected between passes for the required level of completeness. That analysis showed that given a large enough buffer size, any level of completeness is achievable provided that large latencies are acceptable. However, the channel model used for the link was not realistic. Therefore, a better method for determining the required link capacity and spacecraft storage was needed.

The best approach was to characterize the Ka-band link by designing and operating an actual Ka-band telecommunication link from a spacecraft. Until the Mars Reconnaissance Orbiter (MRO) Ka-band Demonstration, this was not possible because either there were problems with the Ka-band signal from the spacecraft (e.g., Mars Observer Ka-band Link Experiment and Mars Global Surveyor Ka-band Link Experiment II) and/or the Deep Space Network (DSN) did not have Ka-band tracking capabilities at Madrid and/or Canberra. Unfortunately, after a very successful cruise phase, the MRO Ka-band equipment failed and even though backup equipment on the spacecraft was available, because of the nature of the failure the experiment was indefinitely postponed [3].

In lieu of an actual spacecraft Ka-band signal, the sky brightness temperature measurements along with models for the DSN Ka-band–capable antennas [4] and MRO's tracking schedule and geometry were used to emulate the Ka-band link for 207 passes (69 passes per Deep Space Communications Complex) for a spacecraft with communications capabilities similar to MRO. The links for Ka-band were designed to be optimal in the expected data return sense [1][5] with at most two data rates per pass subject to a minimum availability requirement (MAR).

In order to compare the performance of Ka-band with 8.41-GHz (X-band), the X-band link was also emulated. This emulation was done both for an optimal X-band link with at most

two data rates subject to a MAR and an X-band link designed for operations above 20 deg elevation with a single data rate that has a margin of at least 1 dB in 90 percent weather.

The purpose of this analysis is threefold. First, the analysis will provide statistics for the outages on the Ka-band link. Even though the link is typically designed for a minimum availability of 85 percent to 90 percent, it has not been clear whether the outages will be of the order of several minutes or several hours. This has implications for the amount of storage the spacecraft will require and for the retransmission schemes that are used. Second, the analysis will determine the power efficacy of the Ka-band relative to X-band in terms of throughput per DC watts used by the RF amplifier on the spacecraft. Finally, the analysis will provide the throughput vs. delay performance of the Ka-band link as well as some guidance on the storage requirements for the spacecraft.

This article is organized as follows. In Section II, assumptions that are used in this article, the emulation setup, and the performance metrics are presented. In Section III, the results are discussed. In Section IV, conclusions are stated.

II. Assumptions and Emulation Setup

Before the link delay-throughput performance could be characterized, assumptions made about the overall system characteristics have to be clarified. These include spacecraft telecommunications parameters, selection of the passes for emulation, link design approach, channel emulation, spacecraft data management, and measures of performance.

A. Spacecraft Telecommunications Parameters

We have selected telecommunications parameters similar to MRO's for our analysis. MRO's Ka-band system has a 35-W RF power traveling-wave tube amplifier (TWTA) transmitting over a 3-m parabolic antenna producing an equivalent isotropic radiated power (EIRP) of 101.3 dBm. The input power consumption of the Ka-band TWTA is 80 W. The X-band system on MRO consists of a 100-W RF power TWTA transmitting over the same 3-m antenna producing an EIRP of 96.2 dBm. The input power to the X-band TWTA is 172 W. Note that the transmitted RF power at X-band is almost three times as great as that for the Ka-band. The reason for this is the fact that, given the available data rates and the geometry considered for this study, the selected RF power levels provide roughly the same performance for both bands.

Both Ka-band and X-band use the same set of data rates shown in Figure 1. These data rates are different than those used on MRO because the coding and data rates used on MRO were designed for its X-band system and actual DSN ground capabilities. As such, the data rates were limited due to spectrum limitations on X-band and limitation on the DSN decoders. In this emulation, there are no such limitations. We have assumed that the spacecraft will use only the (8902,1/6) turbo code for its communications since it has the performance among the available channel codes. The information data rates range from

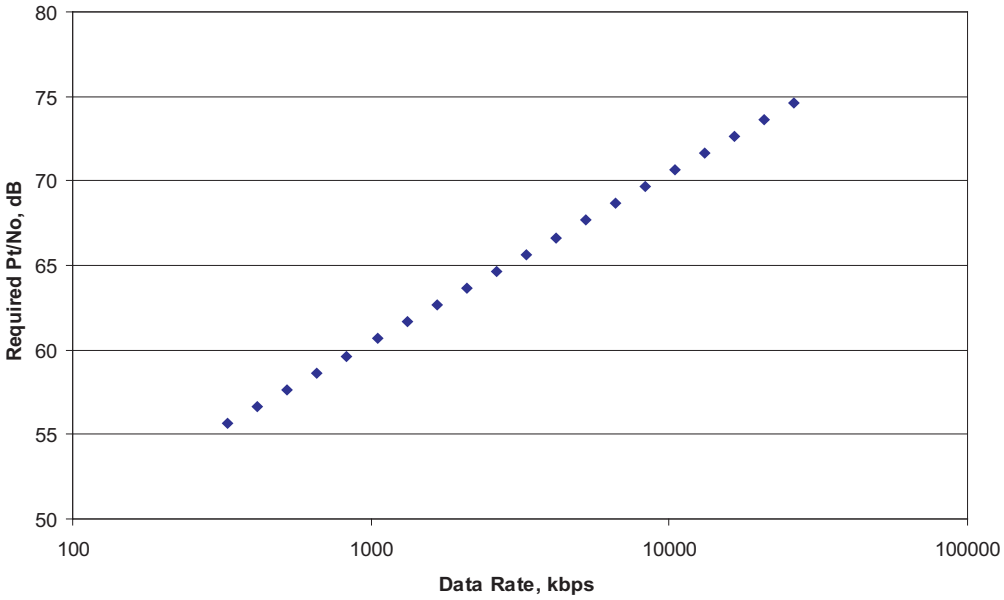

Figure 1. Required P_t/N_0 vs. available data rates.

331 kbps to 26.3 Mbps. The data rates increase in 1 dB intervals. The range of the data rates and the 1 dB separation between them allow the Ka-band link to take maximum advantage of the variation in the link performance due to changes in elevation during a pass for all the passes under considerations.

Even though spacecraft antenna pointing losses could be significant at Ka-band, based on our experience with MRO's Ka-band signal during MRO's cruise phase [3] these pointing losses for MRO are negligible, and therefore are assumed to be zero.

B. Selection of Passes for Emulation

A period from April 1, 2006, through July 31, 2007, was selected for this analysis. Over this period, one pass per week per DSN complex was selected from the MRO DSN schedule. DSN Communications Complexes (DSCCs) are located at Goldstone, California; near Madrid, Spain; and near Canberra, Australia. The passes were selected such that water vapor radiometer/advanced water vapor radiometer (WVR/AWVR) data were available for their entire duration. Because of this, there are weeks during which no passes could be selected for some complexes. In such cases, additional passes were selected from the weeks before and/or after those weeks for the complex. Even though not all the passes selected were originally scheduled on Ka-band–capable 34-m beam waveguide (BWG) antennas, for the purpose of this analysis, parameters for a Ka-band–capable antenna at the selected complex were used. The Ka-band–capable antennas at the DSN are Deep Space Station (DSS) 25 and DSS-26 at Goldstone, DSS-55 at Madrid, and DSS-34 at

Canberra.

C. Optimum Link Design

Both the Ka-band and the X-band links were designed using the approach outlined in [1], [5] and [7]. Under this approach, for each pass, the link is designed with at most two data rates so that the expected pass capacity is maximized subject to a MAR.

To put it mathematically, consider a pass that starts at time t_s and ends at time t_f with an elevation profile $\theta(t)$. Given the tracking station, the spacecraft telecom capabilities, and the distance of the spacecraft to Earth, a given data rate, R_0, has an availability of $F(R_0, \theta_0)$ at elevation θ_0 where

$$F(R_0, \theta_0) = \Pr\{R_s(\theta_0) \geq R_0\} \tag{1}$$

where $R_s(\theta_0)$ is the supportable data rate by the link during the pass at elevation θ_0. Given this, the expected data rate for the link operating with a data rate R_0 at elevation θ_0 is

$$\mathrm{E}[R(\theta_0) | \text{Data rate is } R_0] = R_0 \times F(R_0, \theta_0) \tag{2}$$

Given Equation (2), the expected link capacity of the pass operating with a data rate profile $R(t)$ is given by

$$\mathrm{E}\left[C|_{R(t)}\right] = \int_{t_s}^{t_f} R(t) F(R(t), \theta(t))\, dt \tag{3}$$

The expected data loss during the pass is given by

$$\mathrm{E}\left[L|_{R(t)}\right] = \int_{t_s}^{t_f} R(t)\left(1 - F(R(t), \theta(t))\right) dt \tag{4}$$

and its average availability is given by

$$\mathrm{E}\left[A|_{R(t)}\right] = \frac{1}{t_f - t_s} \int_{t_s}^{t_f} F(R(t), \theta(t))\, dt \tag{5}$$

For a given set of available data rate profiles for a pass, $\mathcal{R}$, the optimum data rate is given by

$$R_{opt}(t) \ni R_{opt}(t) \in \mathcal{R} \text{ and } \mathrm{E}[C|R_{opt}(t)] \geq \mathrm{E}[C|R(t)] \ \forall\ R(t) \in \mathcal{R} \tag{6}$$

Typically, $\mathcal{R}$ is determined by the spacecraft capabilities (e.g., available data rates, coding, onboard computing capabilities, etc.) and by the mission operations guidelines and profile (e.g., limits on the number of data rate changes).

At times, $R_{opt}(t)$ calculated from Equation (6) may not be acceptable because $F(R_{opt}(t), \theta(t))$ may be too low for some time t, $t_s \leq t \leq t_f$. In such cases, the mission can specify a MAR of p, which then limits the set of possible data rate profile to $\mathcal{R}_p$ given by

$$\mathcal{R}_p = \{R(t) | R(t) \in \mathcal{R} \text{ and } F(R(t), \theta(t)) \geq p,\ \forall\ t \in [t_s, t_f]\} \tag{7}$$

and the optimum data rate with MAR of p, $R_{opt}^{(p)}$, is given by

$$R_{opt}^{(p)}(t) \ni R_{opt}^{(p)}(t) \in \mathcal{R}_p \text{ and } \mathrm{E}\left[C|R_{opt}^{(p)}(t)\right] \geq \mathrm{E}\left[C|R(t)\right] \ \forall \ R(t) \in \mathcal{R}_p \tag{8}$$

For our analysis the set $\mathcal{R}$ is limited to those data rate profiles that use at most two of the data rates in Figure 1 and the zero data rate. To put it formally, let $\mathcal{S}$ be the set of data rates in Figure 1, then

$$\begin{aligned} \mathcal{R} \quad = \quad & \Big\{R(t)|R(t) = R_1 \text{ or } R_2, \ R_1 \text{ and } R_2 \in \mathcal{S} \text{ for } t \in \left[t'_s, t'_f\right], \\ & \text{and } R(t) = 0 \text{ for } t \notin \left[t'_s, t'_f\right], \text{ and } \left[t'_s, t'_f\right] \subseteq [t_s, t_f]\Big\} \end{aligned} \tag{9}$$

Note that under this definition, Equation (5) becomes

$$\mathrm{E}\left[A|_{R(t)}\right] = \frac{1}{t'_f - t'_s} \int_{t'_s}^{t'_f} F\left(R(t), \theta(t)\right) dt \tag{10}$$

because availability for data rate zero is meaningless.

MAR values (p) of 10 percent, 50 percent, 65 percent, 80 percent, 85 percent, 90 percent, 92.5 percent, 95 percent, 97.5 percent, and 99 percent are used to evaluate the sensitivity of the link performance to MAR. Monthly zenith atmospheric noise temperature (ZANT) statistics at the three DSCCs for both X-band and Ka-band, along with models for the DSN ground antenna performance parameters [4] and the link geometry, were used to obtain $F\left(R, \theta\right)$ functions for each pass. In this manner, the pass capacity is maximized while the operational complexity is kept to a minimum (through the use of at most two data rates) and a minimum link reliability is maintained.

Depending on the selected MAR, the data rates selected and the times at which the link uses those data rates could change. In Figure 2, this is illustrated for the pass on day 2006-229 occurring over DSS-55. Furthermore, because the weather effects cause greater variations in the performance of Ka-band as a function of elevation and because the EIRP, the ground antenna gain and the space losses are different for X-band and Ka-band, the Ka-band and X-band data rates for the same MAR value are usually not the same. This is illustrated in Figure 3 for the pass over DSS-55 on day 2006-229. In this emulation, occultations of the spacecraft behind Mars and scintillation effects caused by solar conjunction are ignored in order to simplify the analysis.

D. "Current Practice" X-Band Link Design

The link design under the current practice is rather simple. During each pass, the spacecraft is tracked only at elevations greater than 20 deg with a single data rate, R_d. R_d is the highest data rate that provides at least 1 dB of margin at 20 deg elevation in 90 percent weather. To put it mathematically, let $\mathcal{S}$ be the set of data rates in Figure 1, then for each pass we define the set $\mathcal{S}'$ as

$$\mathcal{S}' = \left\{R|R \in \mathcal{S} \text{ and } F\left(R \times 10^{0.1}, 20^\circ\right) \geq 0.9\right\} \tag{11}$$

then R_d is given by

$$R_d = \max_{R \in \mathcal{S}'} R \tag{12}$$

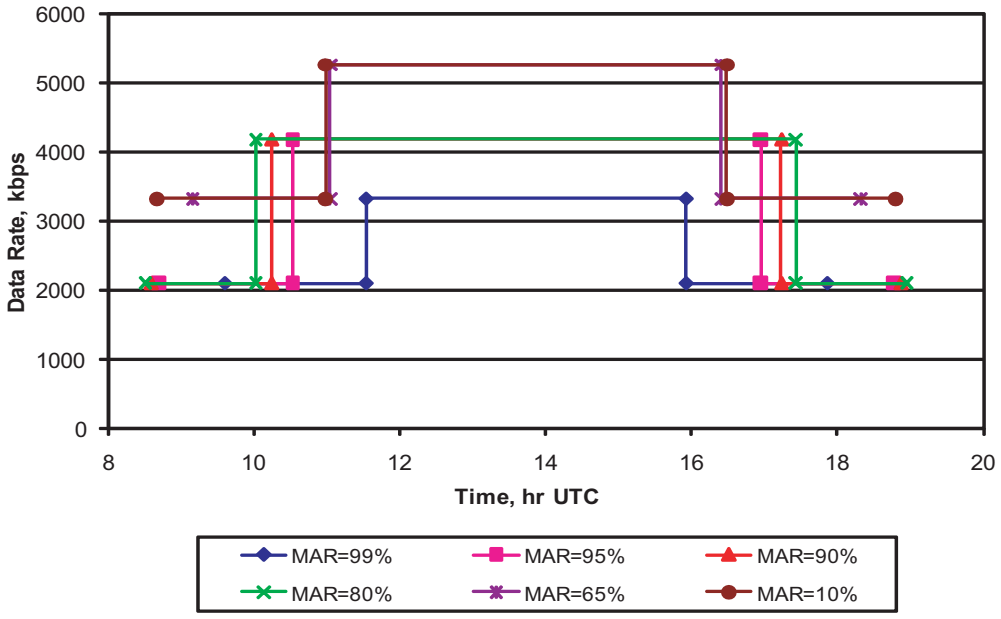

Figure 2. Designed Ka-band data rates for different MAR values, day 2006-229, DSS-55.

E. Channel Emulation

Channel conditions were emulated using the WVR/AWVR data. In order to do so, 31.4-GHz zenith sky brightness temperatures obtained from the WVR/AWVR data were converted to ZANT values at 8.42 GHz and 32 GHz. For each pass, these values were used along with the models for 34-m BWG antenna performance at X-band and Ka-band [4] and the elevation profile for the pass to obtain the actual system gain-to-temperature ratio (G/T) at 1-min intervals. It should be noted that the WVR/AWVR data are provided at intervals of roughly once every 5 min. Therefore, a linear interpolation was used to obtain the ZANT data at 1-min intervals.

Once the actual G/T time series for a pass were obtained, they were compared with the G/T required to close the link. Through this, the status of the link was calculated over the duration of each pass. From the status of the link, the continuity statistics, the data return for each pass, and the amount of data left in the spacecraft buffer after each pass were determined. This is illustrated in Figure 4.

Figure 4 shows the performance of the Ka-band link emulated for day 2006-229 for DSS-55 for a link designed for 90 percent MAR. First, the required G/T is calculated based on the initial link design for 90 percent MAR (the green curve). Note that the required G/T is below the 90 percent predicted G/T (the black curve) indicating that the design meets the minimum availability requirement of 90 percent. Next, the actual G/T is calculated from the WVR/AWVR data (the red curve). Finally, the status of the link is determined with the status being good when the actual G/T is greater than or equal to the required G/T

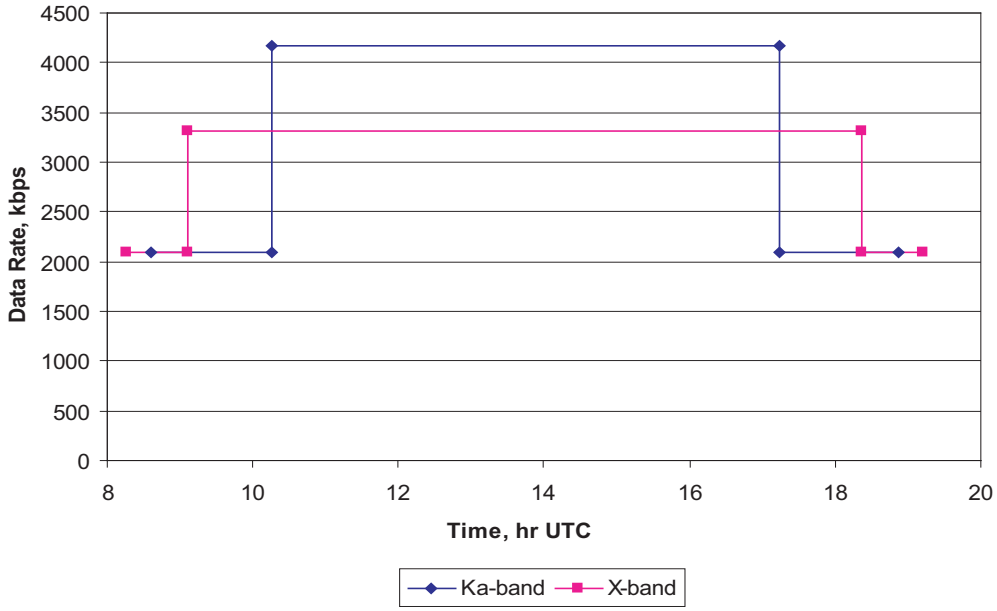

Figure 3. Designed Ka-band and X-band data rates for MAR=90 percent, day 2006-229, DSS-55.

and the status being bad when the actual G/T is less than the required G/T. The status of the link is indicated by the blue curve. From the status curve, the durations of the good periods and bad periods within the pass are calculated. These durations are then collected and are used to calculate the good period and bad period statistics, after all the passes have been emulated. In addition, based on the assumption about data management on the spacecraft (see Section II.F), the amount of data received over the pass and the amount of data left over in the buffer are calculated. Note that this analysis ignores the normal telemetry errors that occur due to additive white gaussian noise in order to simplify the analysis. This methodology is valid because the (8920,1/6) turbo code has an essentially waterfall error rate curve where a few tenths of dBs could make the difference between total data loss and perfect data return.

F. Data Management

Two issues need to be addressed with regards to data management: how much data to collect and what data to transmit. In this analysis, we use the fact that the link design procedure provides the expected pass capacity. From queuing theory, it is well known that in order to keep the amount of data in a queue (the buffer size) finite, it is necessary that the average data input rate for the buffer be less than the average processing rate of the server. Given this, we limit the amount of *new* data collected before a pass to a fraction (less than 1) of the *expected* pass capacity. For example, if this fraction— the data collection factor p_d— is set to 0.95, before a pass with an expected capacity of 1 Gb, only 950 Mb of new data are collected. By varying p_d, the loading of the link is changed and

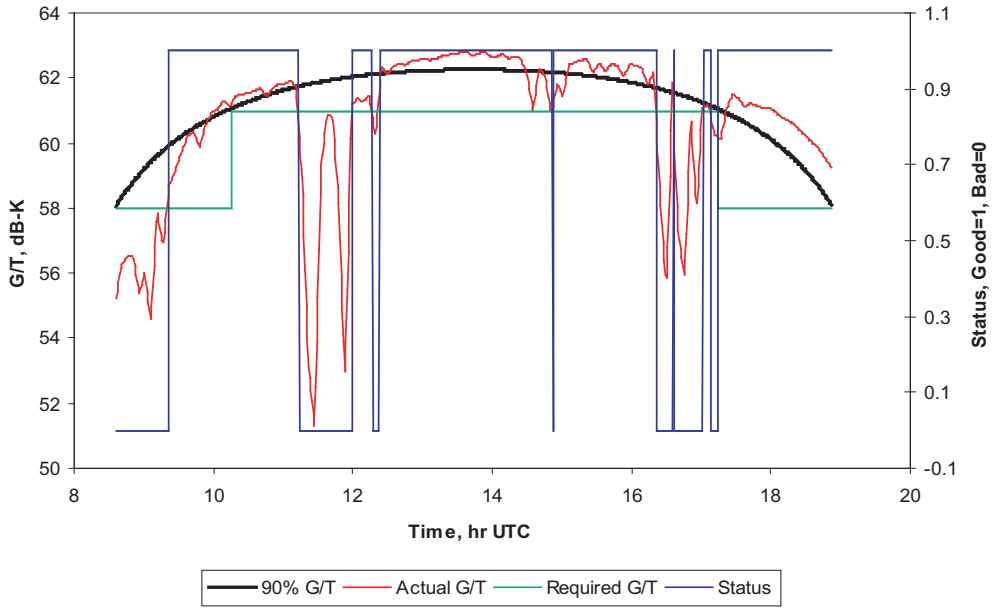

Figure 4. Predicted 90 percent G/T, required G/T, actual G/T and link status, day 2006-229, DSS-55.

thus, delay and throughput of the link will vary. Note that this approach is not that different from current MRO X-band operational practices. MRO reserves 3 percent of its downlink capacity for retransmissions of the data that were not successfully received during previous passes, and the amount of new data collected is equal to 97 percent of the downlink capacity per pass.[1] For the sake of simplicity, in our analysis we assume that no data are collected during a pass as the spacecraft is transmitting.

For data transmission, we assume a slightly modified first-in-first-out (FIFO) policy. Under this approach before the start of the pass, it is known what data will be transmitted during the pass (not in terms of content but rather in terms of their position in the buffer), with the older data transmitted before the newer data. If any of the transmitted data are lost during the pass, retransmission has to occur during subsequent passes. It is assumed that the buffer is purged of all the data that were successfully received during the pass at the end of the pass. This is illustrated in Figure 5.

In Figure 5, some of the data in the buffer are scheduled for transmission during the pass occurring from 12:00 to 20:00. From 12:25 to 14:00, the link suffers an outage that causes the data transmitted during that time not to be received correctly. Therefore, at the end of the pass, the spacecraft is commanded to purge its buffer of the data that were received correctly (the green portion of the data). By the start of the next pass, the data that were not successfully received during the previous pass (the portion of data colored red) are scheduled for transmission first, followed by the data that were in the buffer during the

[1] Author's conversation with Roy Gladden, Jet Propulsion Laboratory, sequencing lead, MRO project.

previous pass but were not transmitted (the cyan data), followed by the new data that were collected after the previous pass (the magenta-colored data). Note that the reception of the data that were not successfully received during the previous pass could be unsuccessful during the next pass. In our analysis, we assume an infinite buffer; therefore, the data are kept in the buffer until they are successfully received on the ground. This approach is different from MRO's approach to data transmission. With MRO, for every pass 97 percent of the downlink capacity is dedicated to the transmission of new data, as opposed to our FIFO scheme.

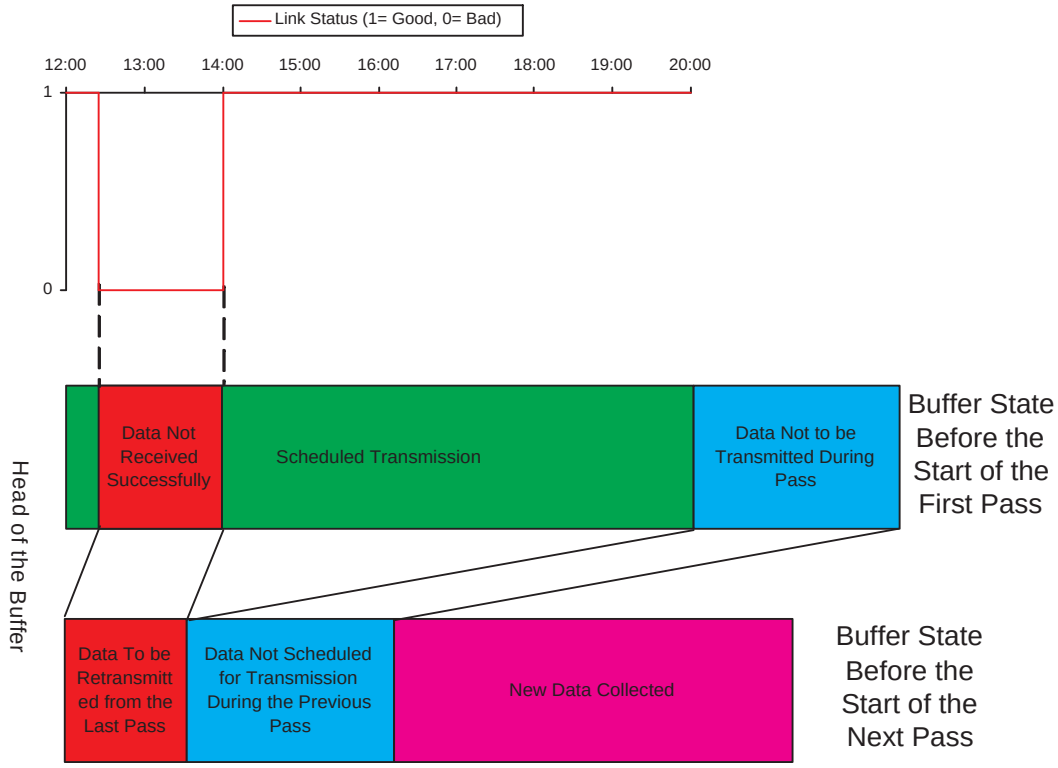

Figure 5. Illustration of the buffer management mechanism.

G. Measures of Performance

1. Capacity and Continuity Metrics

There are several measures of performance by which the capacity and the continuity of the link are evaluated. The following is a brief explanation of these metrics and why they are important:

1. Link capacity and data loss: these metrics are very similar to those obtained by Equations (3) and (4), respectively. For a pass with data rate profile $R(t)$ with start

time t_s and stop time t_f, the link capacity is given by

$$C|_{R(t)} = \int_{t_s}^{t_f} R(t) I_g^{(C)}(t) dt \tag{13}$$

and link data loss is given by

$$L|_{R(t)} = \int_{t_s}^{t_f} R(t) \left(1 - I_g^{(C)}(t)\right) dt \tag{14}$$

where $I_g^{(C)}(t)$ is an indicator function of the link defined as

$$I_g^{(C)}(t) = \begin{cases} 1 & t \text{ belongs to a good period} \\ \\ 0 & \text{otherwise} \end{cases} \tag{15}$$

Note that $\mathrm{E}\left[I_g^{(C)}(t)\right] = F\left(R(t), \theta(t)\right)$.

These two metrics summed either over all passes or over all passes at a single complex give a good picture of the performance of each frequency overall and at each complex. A scheme that has relatively high capacity with tolerable data loss is preferred for science missions. In addition, these two measures allow us to perform trade-offs between different MAR values.

2. Effective data rate: this quantity is obtained by dividing the link capacity by the total track time and could be calculated per pass, per complex, and overall. This measure is especially useful in comparing the performance between complexes because the geometry of the link and the pass schedule could divide the total tracking time unequally among the complexes, thus skewing the data return results. Mathematically, let C_i be the pass capacity obtained for pass i calculated through Equation (13) and T_i be the duration of the time for which the data rate for pass i is non-zero. Note that, because of the way the set of allowable data rate profiles, $\mathcal{R}$, is defined in Equation (9), if pass i starts at time $t_s^{(i)}$ and ends at time $t_f^{(i)}$ then $T_i \leq t_f^{(i)} - t_s^{(i)}$. The per-pass effective data rate is

$$\bar{R}_i = \frac{C_i}{T_i} \tag{16}$$

The overall effective data rate is

$$\bar{R} = \frac{\sum_i C_i}{\sum_i T_i} \tag{17}$$

For a complex, the effective data rate is

$$\bar{R}_{\text{Complex}} = \frac{\sum_{i \in P_{\text{Complex}}} C_i}{\sum_{i \in P_{\text{Complex}}} T_i} \tag{18}$$

where P_{Complex} is the set of all pass indices associated with a given complex.

3. Number of good and bad periods: this metric is important since many retransmission schemes are more concerned with the number of retransmission

requests as opposed to the amount of data retransmitted. Also, in some cases, the outages cause the receiver to go out of lock and the receiver reacquisition times (not taken into account in this study) lead to additional data loss.

4. Number of passes with outages: along with the number of good periods and bad periods, this metric provides information about how good periods and bad periods are distributed among passes.

5. Good period and bad period statistics: this information in the form of average duration and standard deviation is helpful in understanding the nature of outages and good periods.

6. Availability: this quantity is the ratio of the time that the link is in the good state to the total track time. This is the standard measure to which links are designed.

7. "Stability": this is an extension of the idea of availability. Mathematically, stability is defined as

$$\Psi(\tau) = \frac{\sum_{i=1}^{N_g} t_i^{(g)} I_\tau\left(t_i^{(g)}\right)}{t_{tot}} \tag{19}$$

where t_{tot} is the total track time, N_g is the number of good periods observed during that time, $t_i^{(g)}$ is the duration of the ith good period, and $I_\tau(\cdot)$ is an indicator function given by

$$I_\tau(t) = \begin{cases} 1 & t \geq \tau \\ \\ 0 & \text{otherwise} \end{cases} \tag{20}$$

By this definition, $\Psi(\tau)$ is the fraction of time that the link is in a good state of duration greater than or equal to τ. This concept was first introduced in [6]. Availability is $\Psi(0)$.

2. Data Management Metrics

There are two measures of performance that are used to evaluate the data management efficacy:

1. Delay-throughput performance. Since the spacecraft data system could be viewed as a queue, the delay-throughput performance of the system is a natural metric. The delay-throughput performance curve is obtained by plotting the throughput of the system vs. a delay measure. In this case, we use the average delay for the delay measure. Other values that could be used are a fixed percentile delay value such as 95-percentile or 99-percentile delay. These values reflect the maximum delay experienced by 95 percent and 99 percent of the successfully received data,

respectively. Since the passes are scheduled irregularly, the delay is measured in terms of number of passes. Delay-throughput curves are obtained by varying the loading of the system. In this analysis, this is achieved by varying p_d from 0.5 to 1.0 for a given MAR value for both X-band and Ka-band and for the X-band link designed according to the current practice.

2. The maximum of the ratio of the amount of data in storage at the beginning of the pass to the amount of data collected before that pass. This measure is useful because it is a normalized measure. The amount of data in storage on the spacecraft, as measured in number of bits, only relates to specific parameters that are used in this emulation. Through normalization, we can determine how much storage relative to the amount of data that spacecraft collects is needed with Ka-band. This measure also, to some extent, counteracts the variability of the link. Because we are using the actual MRO trajectory for our calculations, over time, the distance between Earth and the spacecraft and the duration and elevation of the passes at each complex vary. These cause variations in the capacity of the link; therefore, the amount of data that are collected before each pass could vary significantly over time. These variations, in turn, could lead to misleading results with regards to the spacecraft storage requirements if no normalization is used. By using a normalized measure, the true effects of the weather on the spacecraft storage requirements could be better assessed. Because of its long name, this quantity is referred to as MRSC (for **M**aximum of **R**atio of the amount of data in **S**torage at the beginning of the pass to the amount of data **C**ollected before that pass).

III. Results

A. Capacity and Data Loss

Figures 6 through 9 show the results for the link capacity and Figures 10 through 13 show the results for the data loss. As seen from these figures, overall, both the Ka-band link and the X-band link perform as expected; however, the performance is not uniform across the complexes. The Ka-band performance is significantly better than expected at Goldstone and significantly worse than expected at Madrid. The Ka-band performance at Canberra is near the expected value. For X-band, the performance is slightly better than expected at Goldstone, slightly worse than expected at Madrid, and near the expected at Canberra. This is to be expected because Ka-band is more sensitive to weather effects than X-band. These results indicate that Goldstone experienced better than average weather; Madrid experienced worse than average weather, and Canberra experienced about average weather during the period of our analysis.

In a site-by-site comparison, Goldstone has the highest expected and actual capacity while Canberra has the lowest. In general, we expect better performance at Goldstone because of its drier climate but we do not expect much disparity between Madrid and Canberra. That this is not the case here is attributed to the fact that the total track time at Madrid is significantly larger than the total track time at Canberra, thus providing less capacity

(see Section III.B for more detail) and the fact that the period under consideration covers more summer months than winter months for Madrid and by the same token, more winter months than summer months for Canberra. Since for Madrid the performance of Ka-band is significantly better during the summer months because of better weather, we expect that Madrid has a higher capacity than Canberra.

Note that for Ka-band as the MAR increases from 10 percent to about 80 percent, the link capacity does not change significantly while the data loss substantially decreases. Therefore, it is recommended to operate the link with a MAR of about 80 percent in order to minimize data outages while obtaining near-maximum capacity. Similarly, for X-band, the capacity does not change substantially as the MAR increases from 10 percent to about 92.5 percent while the data loss noticeably decreases. Therefore, it is recommended that the X-band link be designed with a MAR of 92.5 percent.

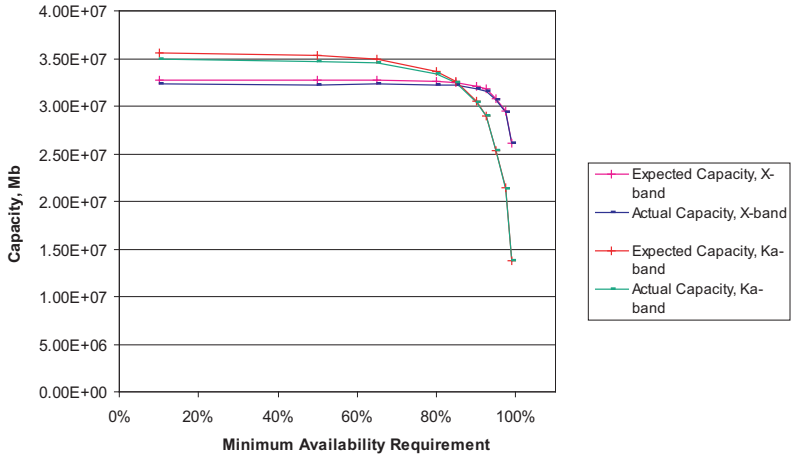

Figure 6. Expected and actual capacity vs. MAR, aggregate.

To compare the capacity and the data loss of the optimized X-band and Ka-band links designed according to the method outlined in Section II.C to the current practice (Section II.D), we selected the X-band link with MAR=92.5 percent and the Ka-band link with MAR=80 percent and compared them with an X-band link designed with a single data rate that is 90 percent available at 20 deg elevation with at least 1 dB of margin. The results are shown in Tables 1 through 5. As seen from these tables, the 92.5 percent X-band and the 80 percent Ka-band have roughly 2 dB advantage over the current practice while producing significantly more loss than the current practice (11.6 dB for 92.5 percent X-band and 16.8 dB more for 80 percent Ka-band). For Ka-band, however, it should be noted that the transmitted RF power and the DC power are significantly lower than those for X-band (30 W and 80 W, respectively, for Ka-band vs. 100 W and 172 W, respectively, for X-band). Once the Ka-band performance is normalized for power, the Ka-band's capacity is significantly higher than X-band's (see Table 2). Similarly, normalized for power, the losses suffered by Ka-band are significantly larger than X-band (see Table 4).

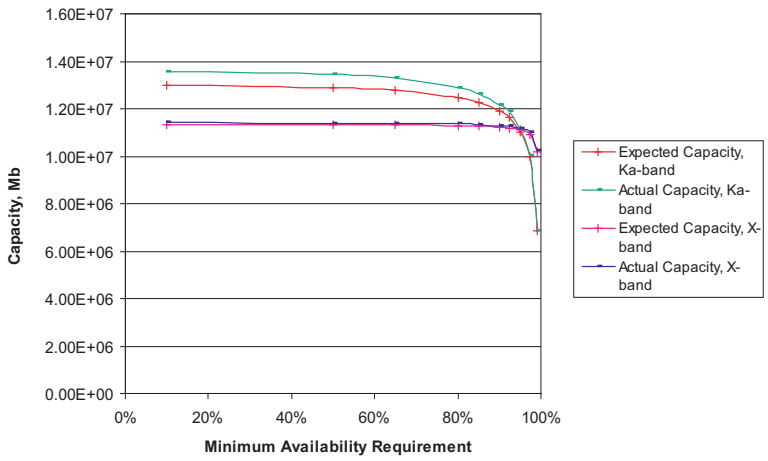

Figure 7. Expected and actual capacity vs. MAR, Goldstone.

The reason that neither data return optimization nor multiple data rates is currently used for X-band can be justified by these results. The 92.5 percent MAR X-band's advantage over the current practice is rather small while its losses are more than an order of magnitude larger. Therefore, it may not be worthwhile to try to optimize the X-band links. With the Ka-band link, however, the link capacity is significantly higher for the same amount of DC power consumed on the spacecraft. Therefore, the link optimization is actually worthwhile.

Note that even with 99 percent MAR, the Ka-band link has significant losses (2.8 dB more, 6.13 dB and 6.03 dB more when normalized for DC and RF power, respectively) while providing almost the same amount of capacity as X-band current practices (1.67 dB less, 1.65 dB and 3.56 dB more when normalized for DC and RF power, respectively; see Table 5). Therefore, because Ka-band will suffer significant losses even under the very stringent 99 percent MAR, retransmission schemes have to be used with Ka-band systems to assure data completeness (see below). Since retransmission is unavoidable with Ka-band, it is recommended that the link design maximizes the expected link capacity and thus, the data return.

B. Effective Data Rate

The effective data rate as a function of MAR is illustrated in Figures 14 to 17. These figures reiterate the observations made about the capacity in the previous subsection: Goldstone has better than expected performance, Madrid has worse than expected performance, and Canberra has near the expected performance. Note that in terms of expected effective data rate, Canberra's effective data rate is closer to Madrid's for Ka-band than is its expected capacity. This is because the Ka-band tracking time for Canberra is significantly less than the Ka-band tracking time for either Madrid or

Table 1. Comparison of actual capacities, current practice, 92.5 percent MAR X-band and 80 percent MAR Ka-band.

	Current Practice, Tb	92.5% X-band, Tb	80% Ka-band, Tb	92.5% X-band Advantage over Current Practice, dB	80% Ka-band Advantage over Current Practice, dB
Aggregate	20.1	31.6	33.4	1.95	2.20
Goldstone	7.01	11.3	12.9	2.06	2.64
Canberra	6.33	9.93	9.79	1.96	1.89
Madrid	6.81	10.4	10.7	1.83	1.98

Table 2. Power-normalized 80 percent MAR Ka-band capacity advantage over 92.5 percent MAR X-band and current practice.

	DC Normalized over Current Practice, dB	DC Normalized over 92.5% X-band, dB	RF Normalized over Current Practice, dB	RF Normalized over 92.5% X-band, dB
Aggregate	5.52	3.57	7.43	5.47
Goldstone	5.96	3.91	7.87	5.81
Canberra	5.22	3.26	7.12	5.17
Madrid	5.30	3.47	7.21	5.38

Table 3. Comparison of actual data losses, current practice, 92.5 percent MAR X-band and 80 percent MAR Ka-band.

	Current Practice, Gb	92.5% X-band, Gb	80% Ka-band, Gb	92.5% X-band Disadvantage over Current Practice, dB	80% Ka-band Disadvantage over Current Practice, dB
Aggregate	70.5	1022	3336	-11.6	-16.8
Goldstone	10.6	93.2	422	-9.45	-16.0
Canberra	26.7	410	1088	-11.9	-16.1
Madrid	33.2	518	1827	-11.9	-17.4

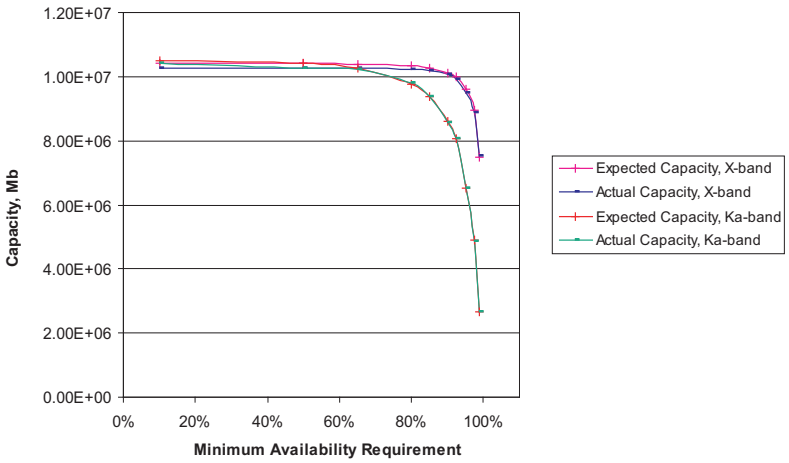

Figure 8. Expected and actual capacity vs. MAR, Canberra.

Table 4. Power-normalized 80 percent MAR Ka-band data loss disadvantage compared to current practice and 92.5 percent MAR X-band.

	DC Normalized vs. Current Practice, dB	DC Normalized vs. 92.5% X-band, dB	RF Normalized vs. Current Practice, dB	RF Normalized vs. 92.5% X-band, dB
Aggregate	-20.1	-8.46	-22.0	-10.4
Goldstone	-19.3	-9.88	-21.2	-11.8
Canberra	-19.42	-7.56	-21.3	-9.46
Madrid	-20.7	-8.80	-22.6	-10.7

Goldstone. This is illustrated in Figure 19.

When comparing the optimized Ka-band's effective data rate performance with the optimized X-band's, we note that for the same MAR, the ratio of effective data rate for Ka-band to the effective data rate for X-band is slightly higher than the ratio of the Ka-band capacity to X-band capacity. This is is because, for the same MAR, X-band total tracking time is higher than Ka-band total tracking time. This is illustrated in Figures 18 through 20. The shorter tracking times for Ka-band, while providing a larger link capacity for the same amount of RF/DC power, provide another advantage for Ka-band in that the ground resources are used less, thus providing the DSN with the capability to support a larger mission set.

Compared to current practices, both X-band and Ka-band optimized links provide significantly higher effective data rates. This is illustrated in Table 6. However, as discussed in the previous subsection, this higher effective data rate comes at the price of

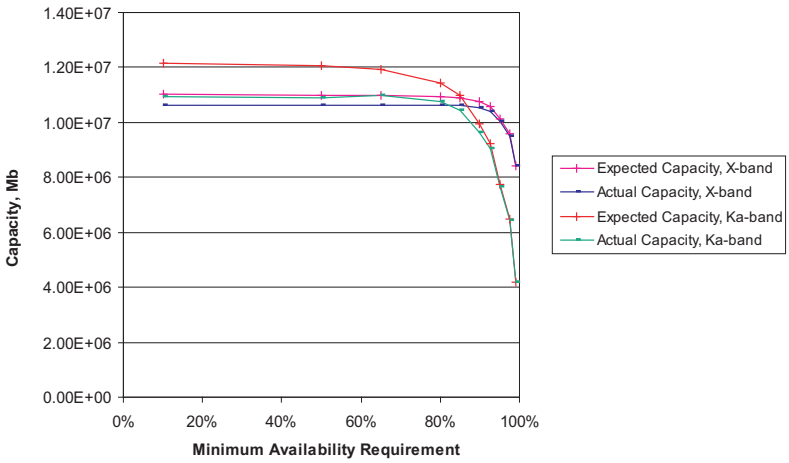

Figure 9. Expected and actual capacity vs. MAR, Madrid.

Table 5. Data loss as a fraction of total data transmitted.

	Current Practice	92.5% MAR X-band	80% MAR Ka-band	99% MAR Ka-band
Aggregate	0.349%	3.13%	9.08%	0.970%
Goldstone	0.151%	0.821%	3.17%	1.22%
Canberra	0.421%	3.97%	10.0%	0.756%
Madrid	0.485%	4.75%	14.5%	1.07%

having higher data losses.

Finally, since the effective data rate depends on the total tracking time, it is also instructive to compare the total tracking time of the current practices for this case with the total tracking time of optimized X-band and Ka-band links. This is illustrated in Table 7. As seen from this table, the 80 percent Ka-band link has a shorter tracking time than the 92.5 percent X-band tracking time but longer than the current practices.

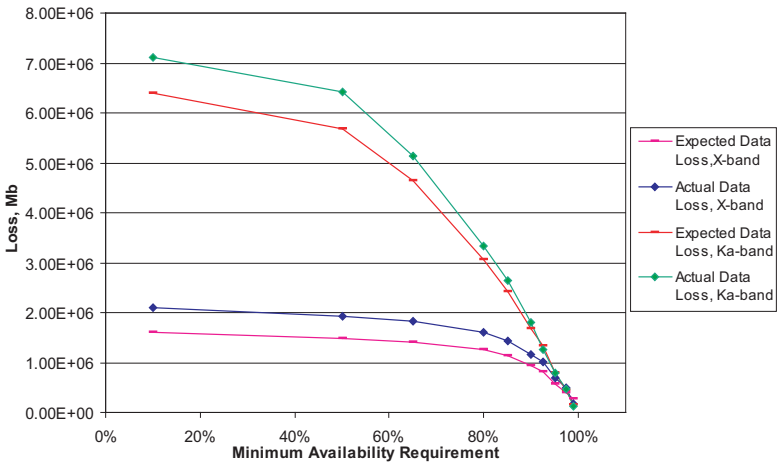

Figure 10. Expected and actual data loss vs. MAR, aggregate.

Table 6. Actual effective data rates.

	Current Practice, Mbps	92.5% MAR X-band, Mbps	80%MAR Ka-band, Mbps
Aggregate	3.70	5.11	5.70
Goldstone	3.76	5.34	6.42
Canberra	3.64	5.06	5.30
Madrid	3.71	4.92	5.36

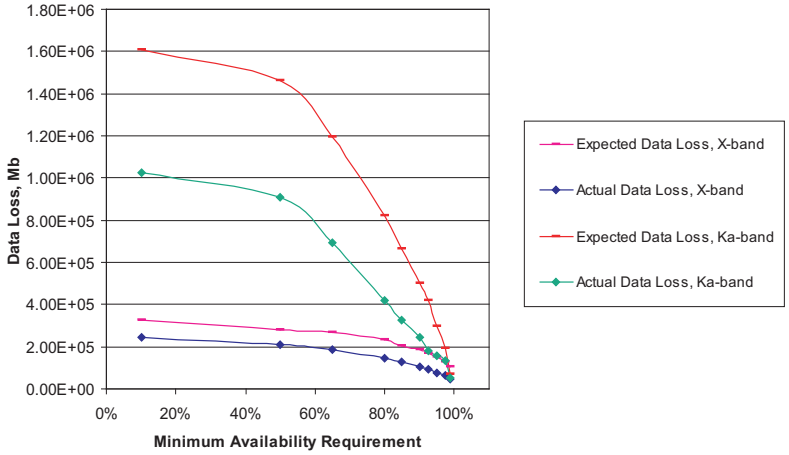

Figure 11. Expected and actual data loss vs. MAR, Goldstone.

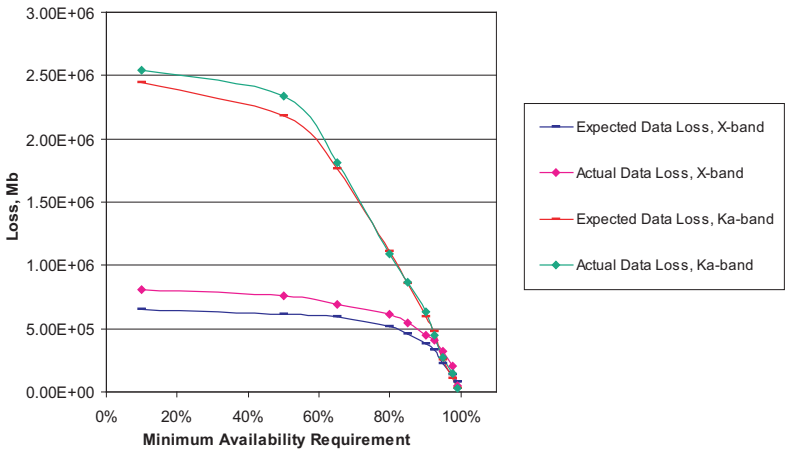

Figure 12. Expected and actual data loss vs. MAR, Canberra.

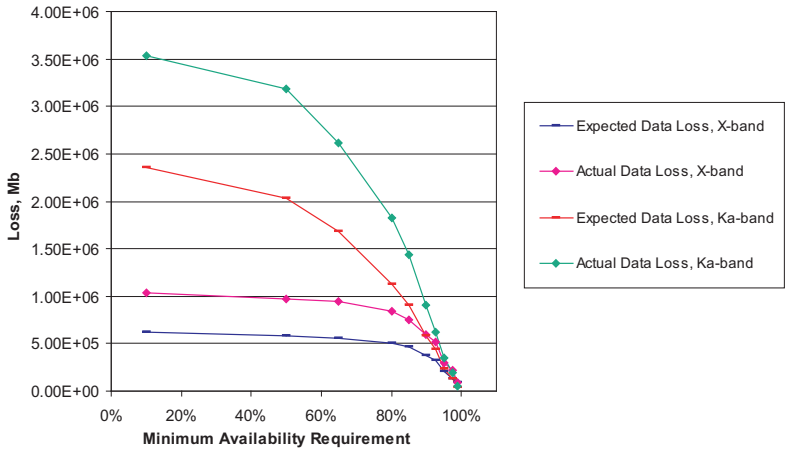

Figure 13. Expected and actual data loss vs. MAR, Madrid.

Table 7. Tracking times.

	Current Practice, hr	92.5% MAR X-band, hr	80% MAR Ka-band, hr
Aggregate	1512.4	1718.2	1627.6
Goldstone	518.68	586.22	557.43
Canberra	483.48	545.52	513.00
Madrid	510.18	586.47	557.18

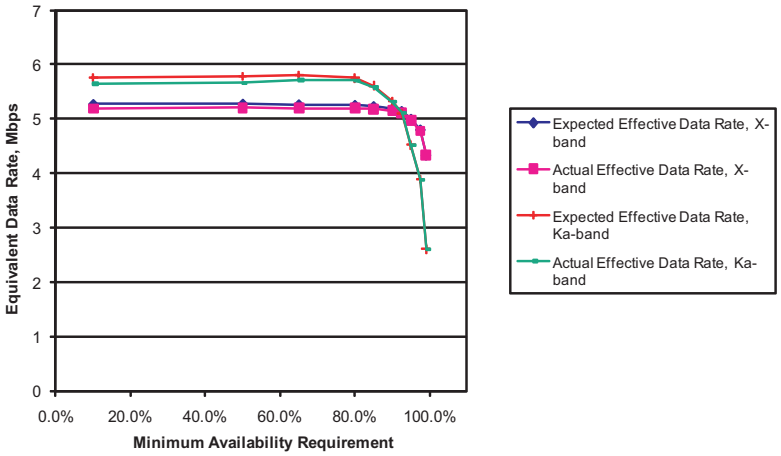

Figure 14. Expected and actual effective data rate vs. MAR, aggregate.

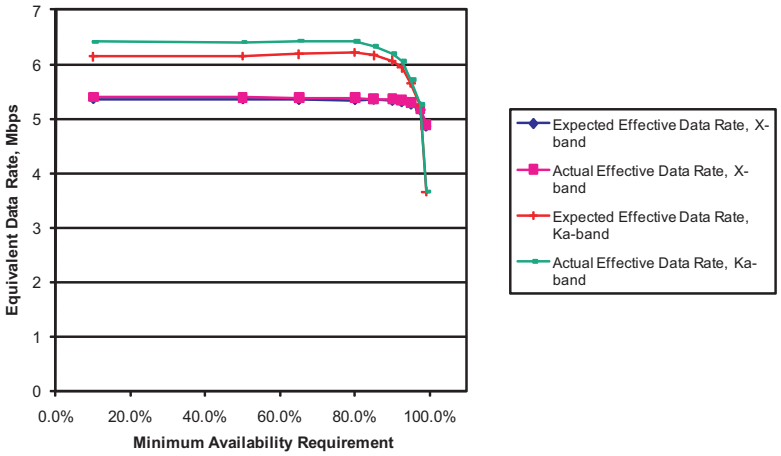

Figure 15. Expected and actual effective data rate vs. MAR, Goldstone.

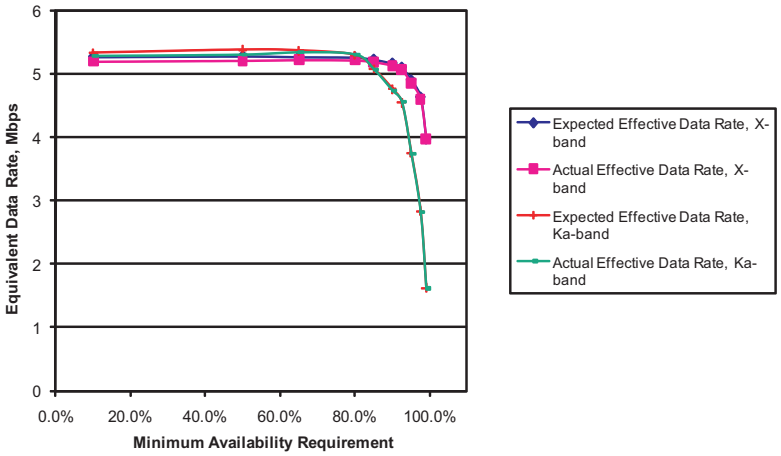

Figure 16. Expected and actual effective data rate vs. MAR, Canberra.

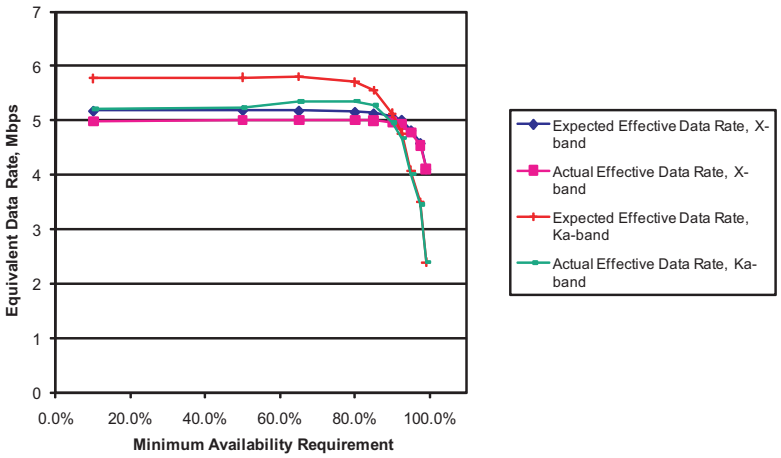

Figure 17. Expected and actual effective data rate vs. MAR, Madrid.

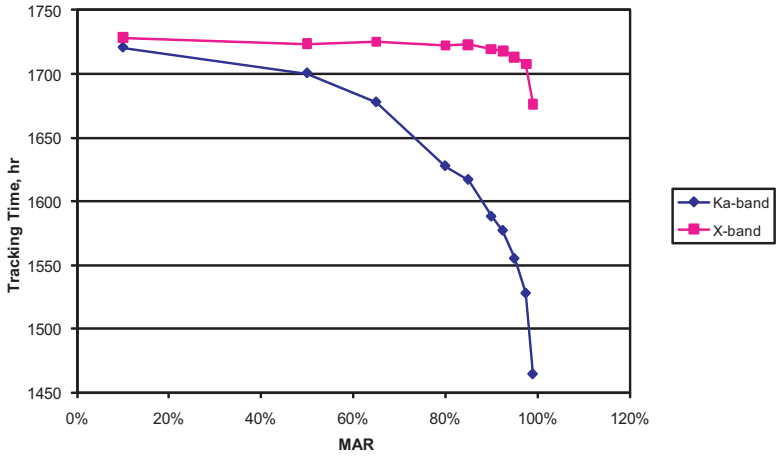

Figure 18. Total tracking time, X-band and Ka-band, aggregate.

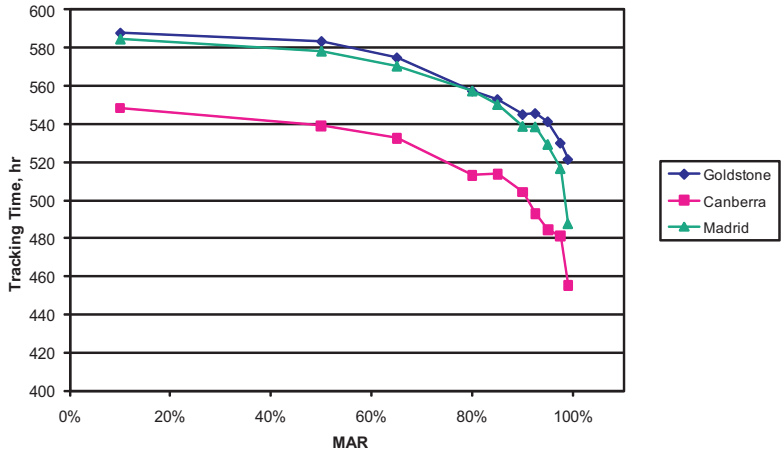

Figure 19. Ka-band tracking times vs. MAR by complex.

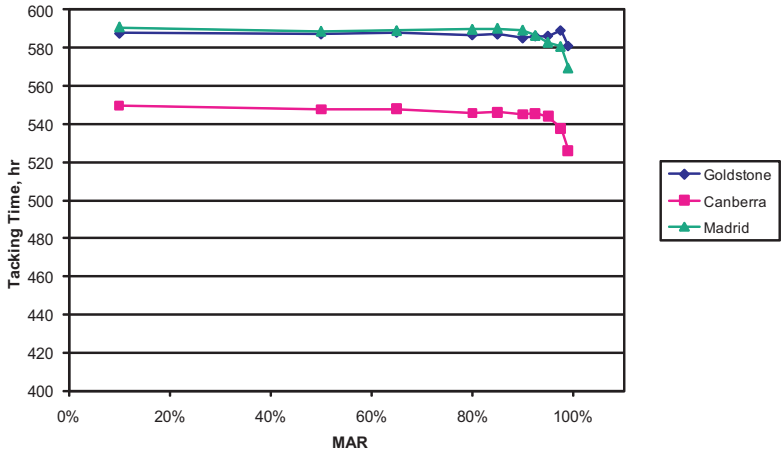

Figure 20. X-band tracking times vs. MAR by complex.

C. Number of Good and Bad Periods and Number of Passes with Outages

The number of good periods and bad periods and the number of passes with outages (bad periods) are plotted as functions MAR in Figures 21 through 24. As seen from these figures, the number of passes with outages for both X-band and Ka-band are roughly the same for the same MAR values; however, the number of bad periods (and consequently good periods) are greater for Ka-band than for X-band. This is to be expected. The analysis performed here covers the same time period for X-band as it does for Ka-band. Given this, when Ka-band experiences bad weather, so does X-band; however, since the weather effects are more severe for Ka-band than for X-band, Ka-band experiences a larger number of outages. Note that as the MAR increases, the difference between the number of bad periods for Ka-band and the number of bad periods for X-band decreases.

Looking at the performance of each complex, we observe that Goldstone has the fewest number of bad periods and the fewest number of passes with bad periods and Madrid has the most number of bad periods and the most number of passes with bad periods for both X-band and Ka-band. Madrid has more than half the bad periods and half the passes with bad periods for a given MAR for Ka-band. For X-band, Madrid has a plurality of both the number of passes with bad periods and the number of bad periods. As Figures 21 through 24 indicate, for Ka-band, a large fraction of all passes suffer some sort of outage. Therefore, these results indicate that a data management scheme using retransmissions is imperative for efficient operation of the Ka-band link.

Compared to the current practices, both the optimized X-band link and the optimized Ka-band link suffer more outages. This is shown in Table 8. As seen from this table, only 16 passes (about one seventh of all passes) suffer any losses under the current practice, while optimized 92.5 percent MAR X-band has 52 passes (about one fourth of all passes) and optimized 80 percent MAR Ka-band has 78 passes (more than one third of all passes) that suffer losses. It is notable that under the current practice, still one seventh of all passes suffer some sort of weather outage. However, the total number of bad periods is substantially smaller under the current practice than either the optimized 92.5 percent MAR X-band or the optimized 80 percent MAR Ka-band.

D. Good and Bad Period Statistics

The good period average and standard deviations are shown in Figures 25 through 28 The bad period average and standard deviations are shown in Figures 29 through 32. The good period statistics indicate that, in general, as the MAR increases, the good period average also increases. The only exception to this is Canberra where, in all likelihood, the drop in the average good period duration is caused by the limitations on the total tracking time that the higher MAR values impose (see Section III.B). The standard deviation of good periods tends to increase slightly or remain constant until the MAR approaches 92.5 percent and then it decreases. This is explained by the fact that as the MAR increases, the number of weather events that cause outages over short periods of time (thus increasing the number of both good and bad periods) decreases relative to the

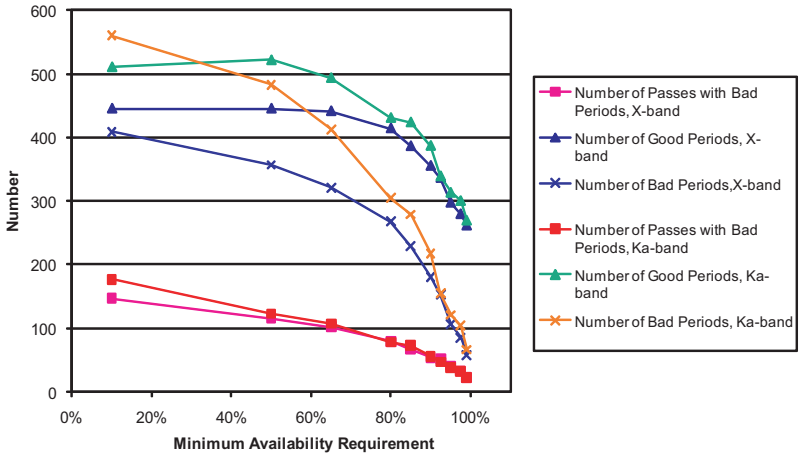

Figure 21. Number of good periods and bad periods and number of passes with outages, X-band and Ka-band, aggregate.

Table 8. Number of good periods and bad periods and number of passes with bad periods (bad passes), current practice, 92.5 percent MAR X-band and 80 percent MAR Ka-band.

	Current Practices			92.5% MAR X-band			80% MAR Ka-band		
	Good	Bad	Bad Passes	Good	Bad	Bad Passes	Good	Bad	Bad Passes
Aggregate	230	27	16	336	153	52	431	305	78
Goldstone	73	5	3	91	27	10	109	57	13
Canberra	77	9	4	96	37	18	134	87	27
Madrid	80	13	9	149	89	24	188	161	38

number of weather events that cause outages over longer periods of time. This in turn results in an increase in the good period standard deviation. Comparing X-band good periods with Ka-band good periods, we notice that X-band good periods have in general longer averages and larger standard deviations than Ka-band. However, both the average good period curve and the good periods standard deviation curve for X-band and Ka-band have similar shapes. As for statistics themseleves, the average good period for Ka-band even with a MAR of 10 percent is nearly 3 hr.

The bad period statistics are not as well-behaved as the good period statistics. This could be partially because there are fewer bad periods than good periods, thus producing more varying results. Overall, the Ka-band bad period averages and standard deviations are greater than those of X-band for the same MAR value. There is a difference in the shape of the curves for these metrics between X-band and Ka-band. In addition, for Ka-band the shape of these curves varies from complex to complex. Note that the shape of the

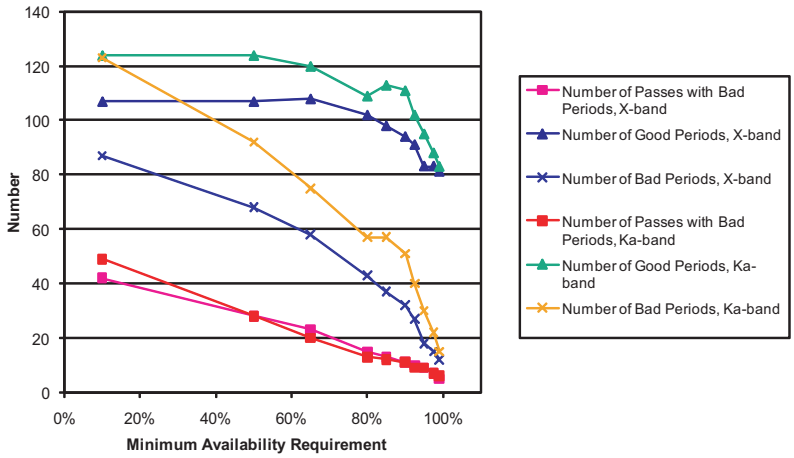

Figure 22. Number of good periods and bad periods and number of passes with outages, X-band and Ka-band, Goldstone.

aggregate curves (Figure 29) is very similar to those for Madrid (Figure 32). This is because Madrid has about half the bad periods for both X-band and Ka-band and its statistics dominate the aggregate curve. While the differences in the good and bad period statistics could be caused by worse than expected weather at Madrid, there may also be differences in the overall weather patterns among the complexes. Finally, these differences among complexes could be affected by geometry, link design, and seasons. Further study is necessary.

The bad period statistics indicate that the aggregate average Ka-band bad period is about half an hour or less with the standard deviation of about 1 hr. That means that 95 percent of the time, a bad period is less than 2.5 hr. However, this is not the case for all complexes. For Canberra, the bad period average and standard deviation see a significant increase for MAR values between 85 percent and 95 percent. For Goldstone, the bad period averages for both X-band and Ka-band increase slightly with MAR, while the standard deviation has an irregular shape with the higher MAR values, in general experiencing smaller standard deviations than the lower MAR values. Again, these differences could be caused by a fundamental difference in the weather patterns among the complexes, by an artifact of the geometry of the passes, or by the link design approach, or by a combination of all these factors. Further investigation is warranted.

Comparing the performance of the optimized X-band and Ka-band links to the current practice indicates that under the current practice, as expected, on the average the good periods are longer and the bad periods are shorter than either the optimized 92.5 percent MAR X-band or the optimized 80 percent MAR Ka-band. Furthermore, under the current practice, the standard deviations of good periods and bad periods are smaller than those of the optimized 92.5 percent MAR X-band and the optimized 80 percent MAR Ka-band (see Tables 9 and 10).

Table 9. Average and standard deviations of good periods, current practice, optimized 92.5 percent MAR X-band and optimized 80 percent MAR Ka-band.

	Current Practice		92.5% MAR X-band		80% MAR Ka-band	
	Average, hr	Standard Dev., hr	Average, hr	Standard Dev., hr	Average, hr	Standard Dev., hr
Aggregate	6.55	2.83	4.96	3.96	3.44	3.52
Goldstone	7.09	2.43	6.38	3.72	4.94	3.70
Canberra	6.26	3.09	5.51	3.84	3.53	3.52
Madrid	6.34	2.84	3.75	3.81	2.52	3.07

Table 10. Average and standard deviations of bad periods, current practice, optimized 92.5 percent MAR X-band and optimized 80 percent MAR Ka-band.

	Current Practice		92.5% MAR X-band		80% MAR Ka-band	
	Average, hr	Standard Dev., hr	Average, hr	Standard Dev., hr	Average, hr	Standard Dev., hr
Aggregate	0.217	0.217	0.330	0.519	0.470	0.853
Goldstone	0.217	0.142	0.196	0.253	0.332	0.483
Canberra	0.194	0.193	0.457	0.730	0.467	0.858
Madrid	0.233	0.252	0.317	0.459	0.521	0.942

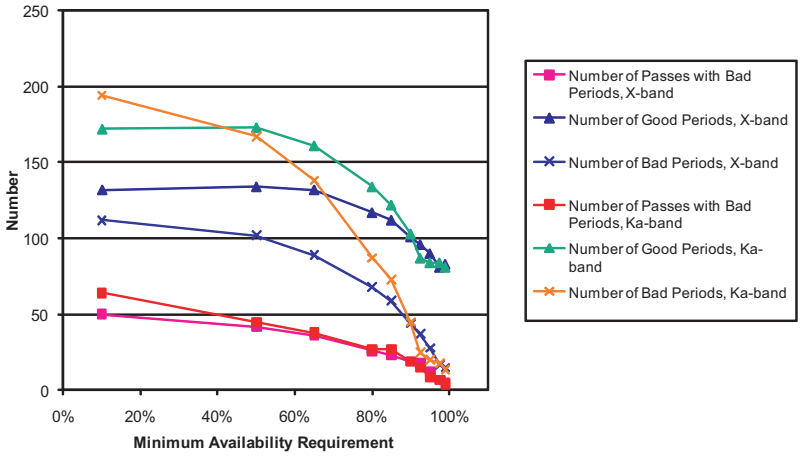

Figure 23. Number of good periods and bad periods and number of passes with outages, X-band and Ka-band, Canberra.

E. Availability

The expected and the actual link availabilities are shown in Figures 33 through 36. As seen from these figures, the aggregate availability of both X-band and Ka-band matches the expected availability, but on a per-complex basis, the actual availability does not match the expected availability. Similar to the results for link capacity and equivalent data rates (Sections III.A and III.B), Goldstone has a higher availability than expected, Madrid has a lower availability than expected, and Canberra has an availability slightly better than expected.

When comparing the optimized performance with the current practice, we notice that under the current practice, the link has substantially higher availability than under the optimized links. This is shown in Table 11. As seen from this table, under the current practice, the link is available more than 99 percent of the time at all complexes while it is available only 97.5 percent of the time with optimized 92.5 percent MAR X-band and 91.6 percent of the time with the optimized 80 percent MAR Ka-band. Note that even though for the X-band and the Ka-band optimized links, the MAR is 92.5 percent and 80 percent, respectively, the actual availability of the link is greater than these values. This is because MAR is a lower limit on the expected instantaneous availability of the link and therefore, the expected instantaneous availability of the link is always greater than the MAR for which it is designed.

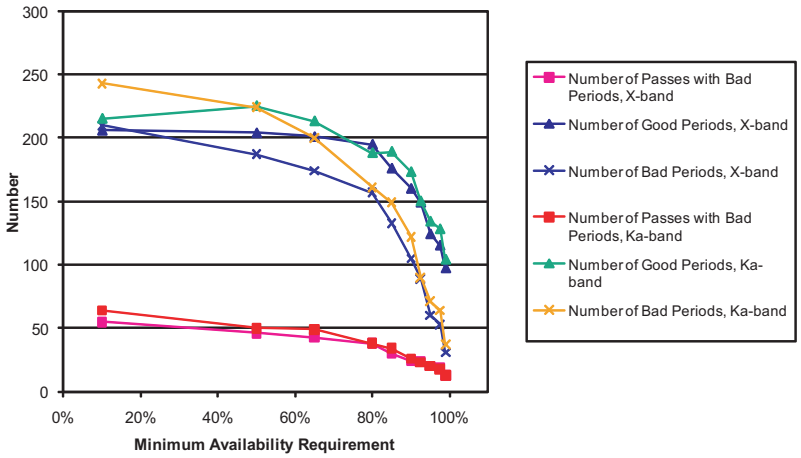

Figure 24. Number of good periods and bad periods and number of passes with outages, X-band and Ka-band, Madrid.

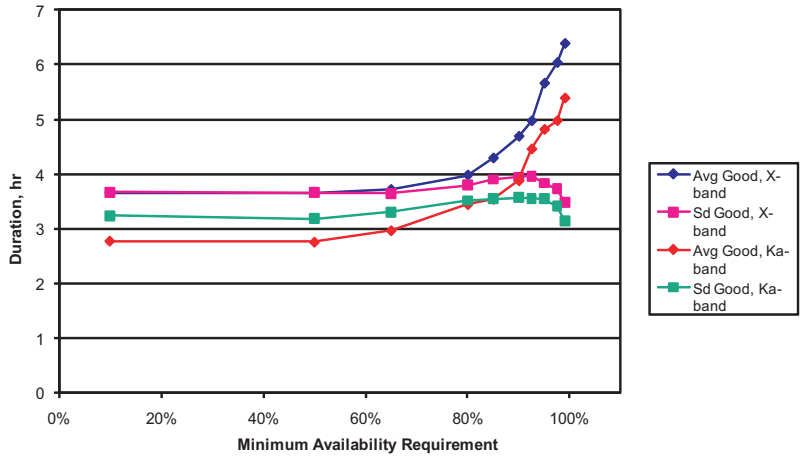

Figure 25. Good period statistics, X-band and Ka-band, aggregate.

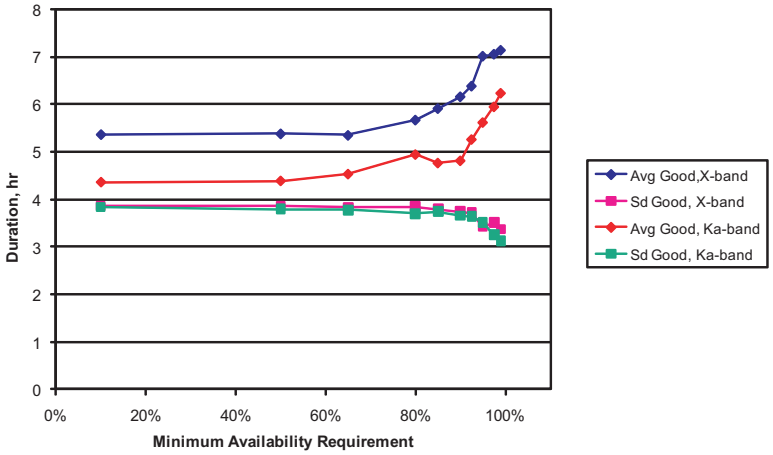

Figure 26. Good period statistics, X-band and Ka-band, Goldstone.

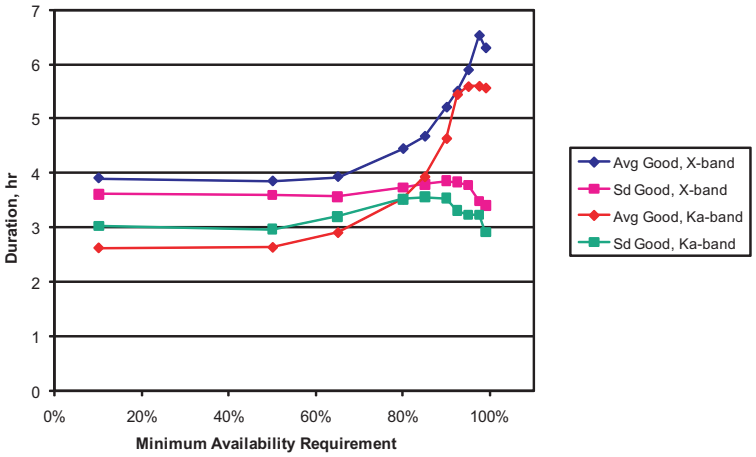

Figure 27. Good period statistics, X-band and Ka-band, Canberra.

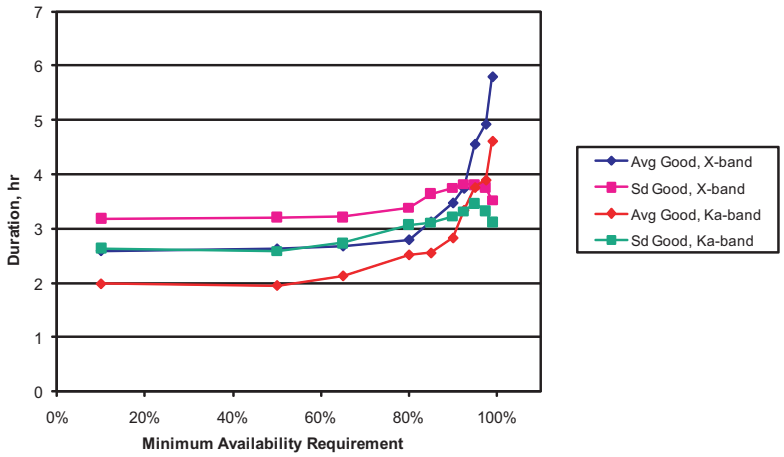

Figure 28. Good period statistics, X-band and Ka-band, Madrid.

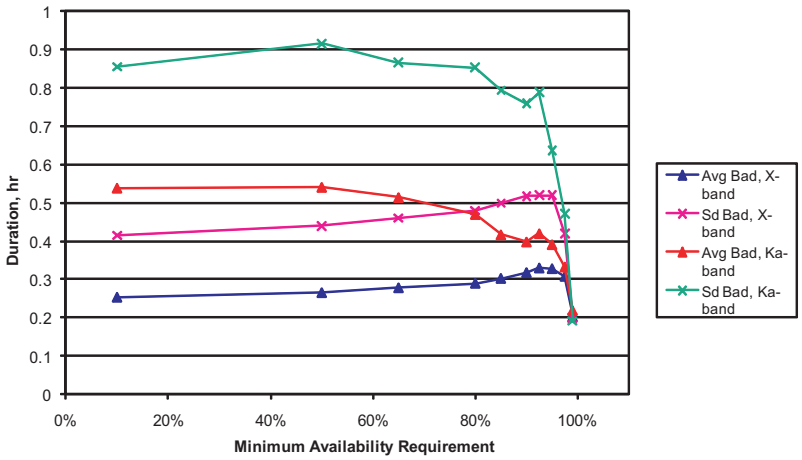

Figure 29. Bad period statistics, X-band and Ka-band, aggregate.

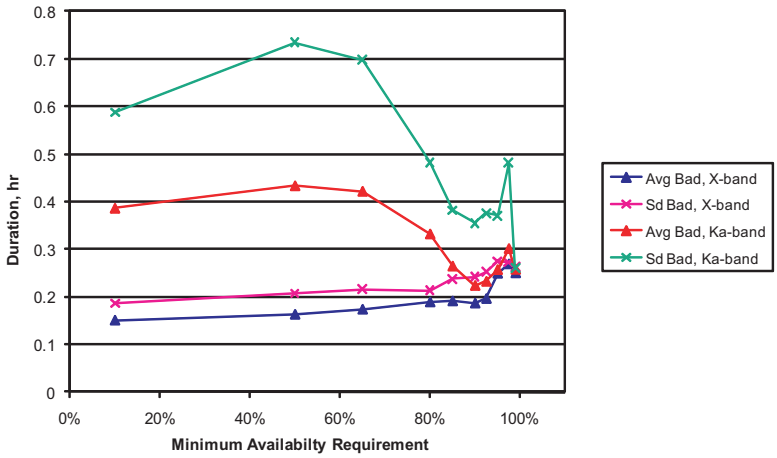

Figure 30. Bad period statistics, X-band and Ka-band, Goldstone.

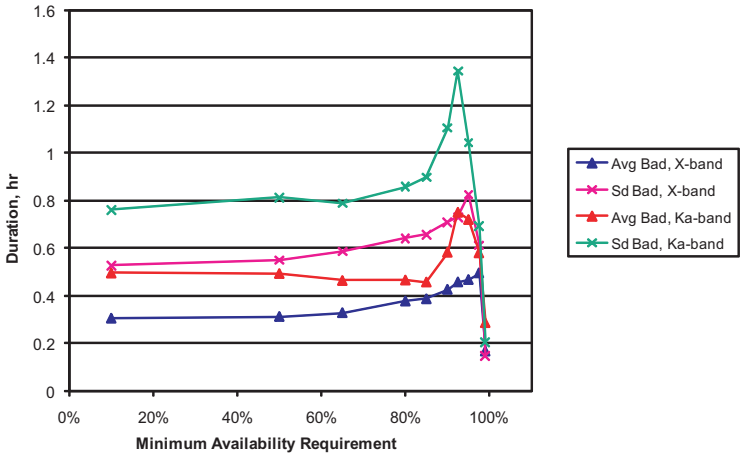

Figure 31. Bad period statistics, X-band and Ka-band, Canberra.

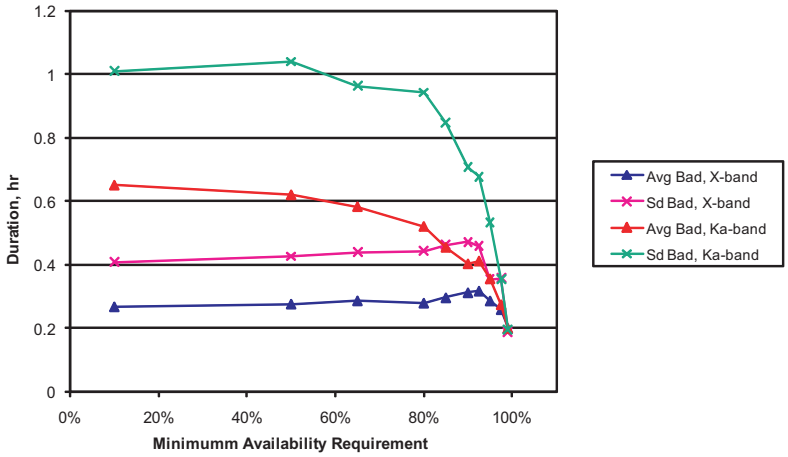

Figure 32. Bad period statistics, X-band and Ka-band, Madrid.

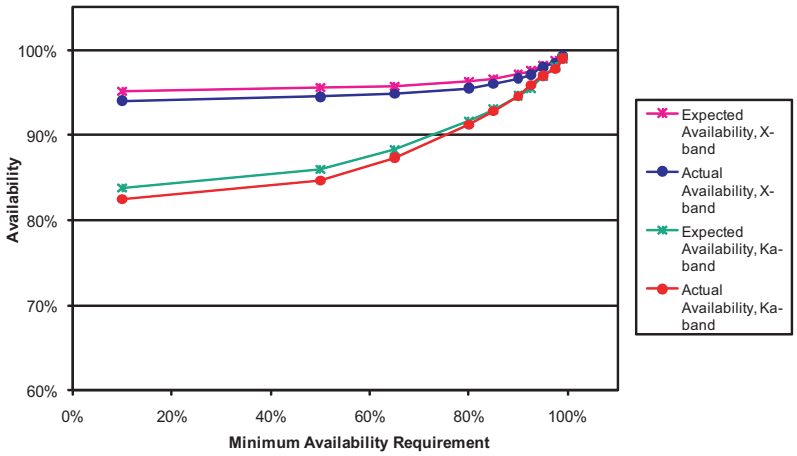

Figure 33. Expected and actual availability, X-band and Ka-band, aggregate.

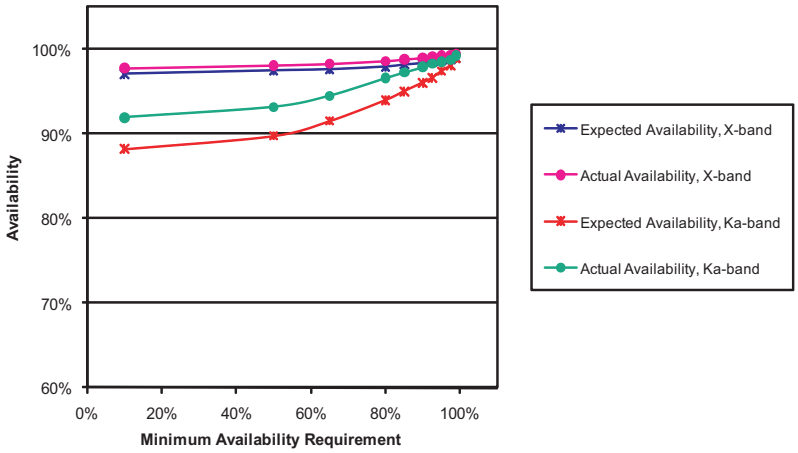

Figure 34. Expected and actual availability, X-band and Ka-band, Goldstone.

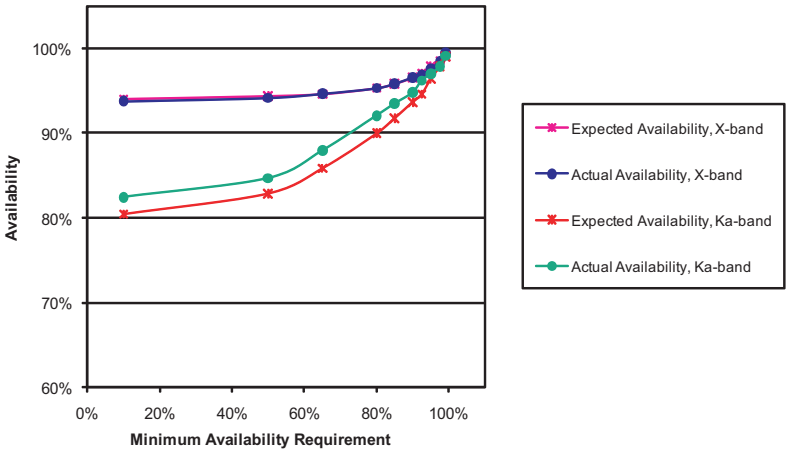

Figure 35. Expected and actual availability, X-band and Ka-band, Canberra.

Table 11. Comparison of expected and actual availabilities, current practice, optimized 92.5 percent MAR X-band and optimized 80 percent MAR Ka-band.

	Current Practice		92.5% MAR X-band		80% MAR Ka-band	
	Expected	Actual	Expected	Actual	Expected	Actual
Aggregate	>99%	99.6%	97.5%	97.1%	91.6%	91.2%
Goldstone	>99%	99.8%	98.5%	99.1%	94.0%	96.6%
Canberra	>99%	99.6%	97.0%	96.9%	90.0%	92.1%
Madrid	>99%	99.4%	97.0%	95.2%	90.6%	85.0%

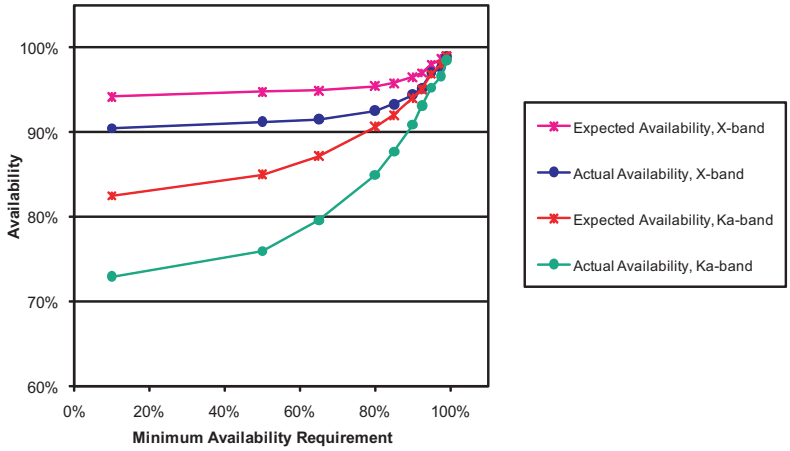

Figure 36. Expected and actual availability, X-band and Ka-band, Madrid.

F. Stability

The 30-min, 1-hr and 3-hr stabilities for optimized Ka-band and X-band links as functions of MAR are plotted in Figures 37 to 44. As seen from these figures, for the same MAR value, the X-band link is more stable than the Ka-band link. Overall, the 3-hr stability for X-band is at least 80 percent but for Ka-band it is only 65 percent. Overall, the 30-min stability is at least 92 percent for X-band and 80 percent for Ka-band. On a per-complex basis, Madrid has the least stability while Goldstone has the most stability for both X-band and Ka-band. This result is consistent with the results described in the previous sections. As expected, in general, as the MAR increases the link becomes more stable. Canberra Ka-band data (Figure 41) shows a slight deviation from this general trend. For Canberra Ka-band there is a slight decrease in stability going from 95 percent MAR to 97.5 percent MAR. This is caused by the decrease in the track times of some passes for Ka-band at Canberra as the MAR increases.

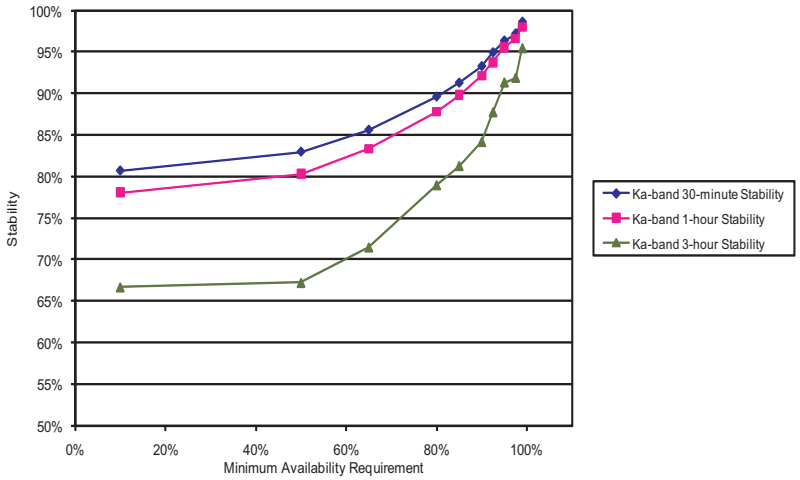

Figure 37. Ka-band stability, 30-min, 1-hr and 3-hr, aggregate.

Comparing the stability of the current practice to the optimized link, we see that the link is far more stable under the current practice. This is shown in Figures 45 through 48. As seen from these figures, overall, the 4-hr stability of the link under the current practice is better than 94 percent. By contrast, for 92.5 percent MAR X-band and 80 percent MAR Ka-band, the aggregate 4-hr stability is 87 percent and 76 percent, respectively. Even at the worst complex (Madrid) the link is more stable under the current practice. The 4-hour stability for Madrid is 91 percent under the current practice, 81 percent for 92.5 percent MAR X-band and 65 percent for 80 percent MAR Ka-band.

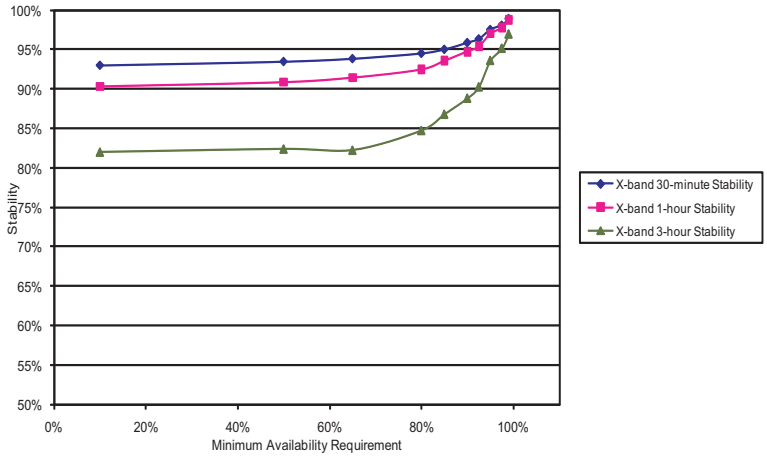

Figure 38. X-band stability, 30-min, 1-hr and 3-hr, aggregate.

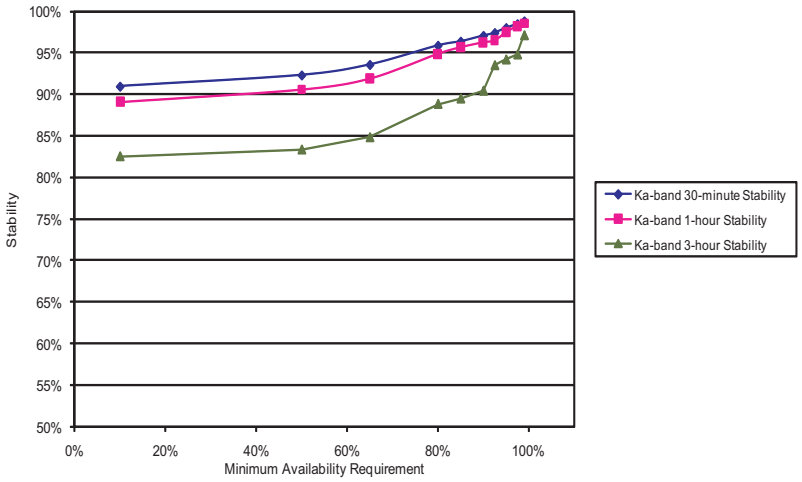

Figure 39. Ka-band stability, 30-min, 1-hr and 3-hr, Goldstone.

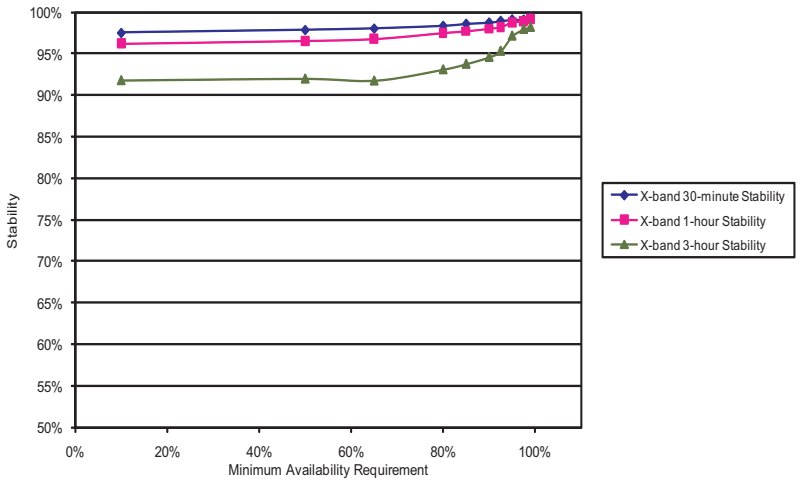

Figure 40. X-band stability, 30-min, 1-hr and 3-hr, Goldstone.

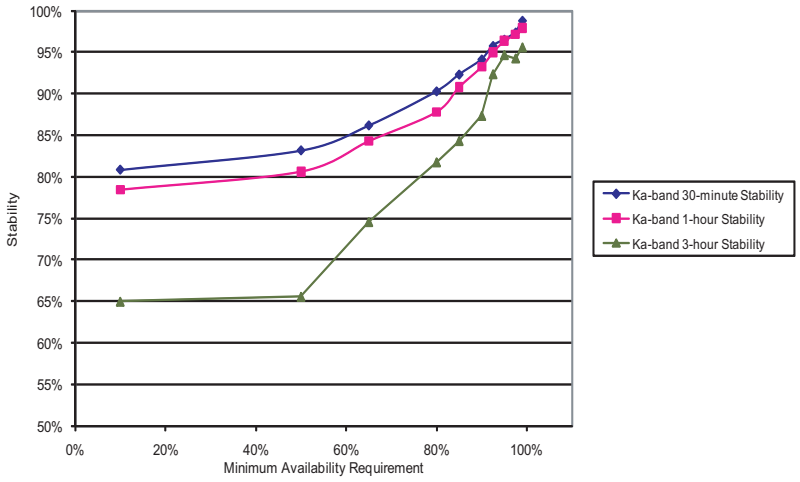

Figure 41. Ka-band stability, 30-min, 1-hr and 3-hr, Canberra.

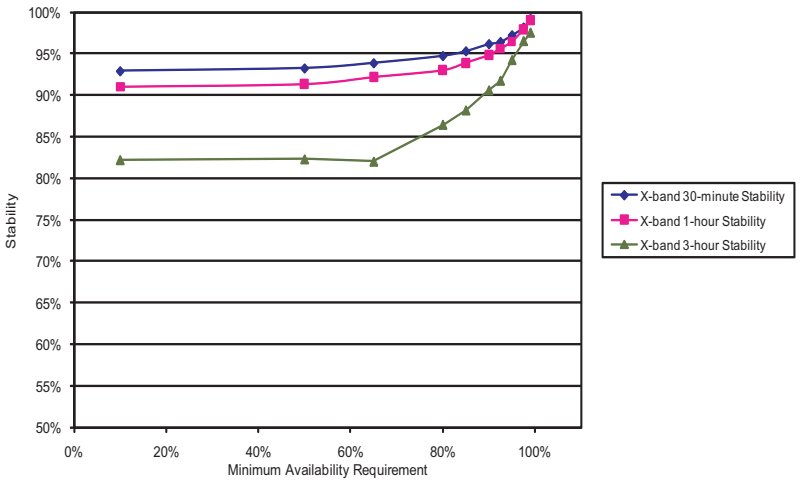

Figure 42. X-band stability, 30-min, 1-hr and 3-hr, Canberra.

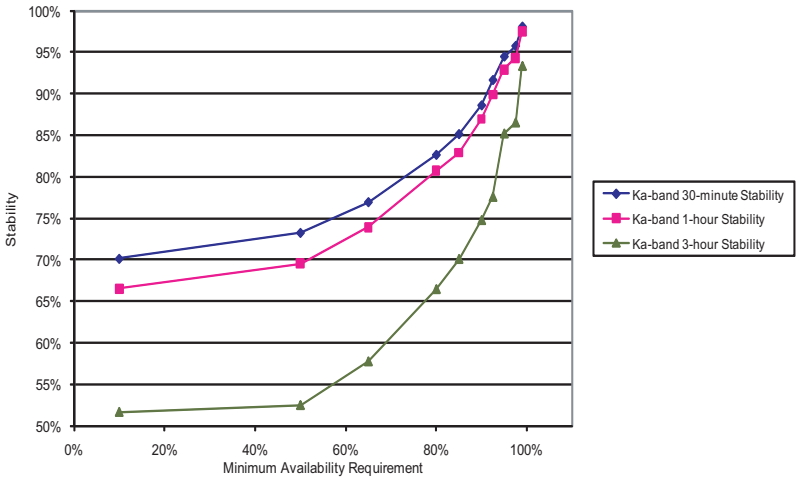

Figure 43. Ka-band stability, 30-min, 1-hr and 3-hr, Madrid.

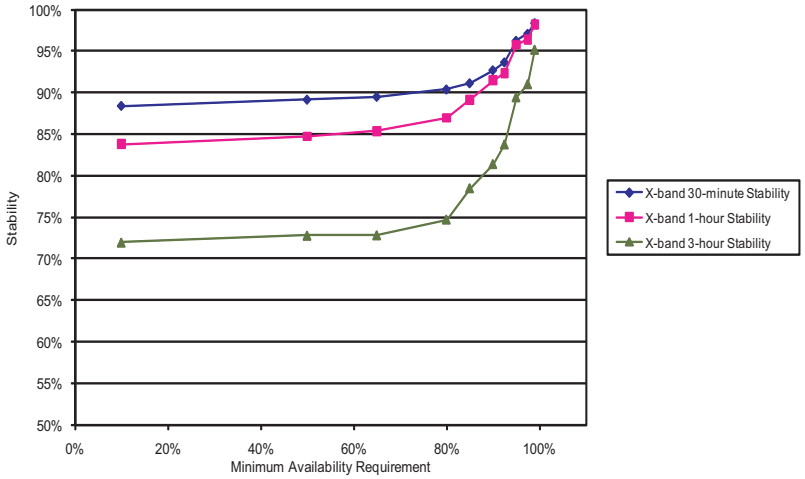

Figure 44. X-band stability, 30-min, 1-hr and 3-hr, Madrid.

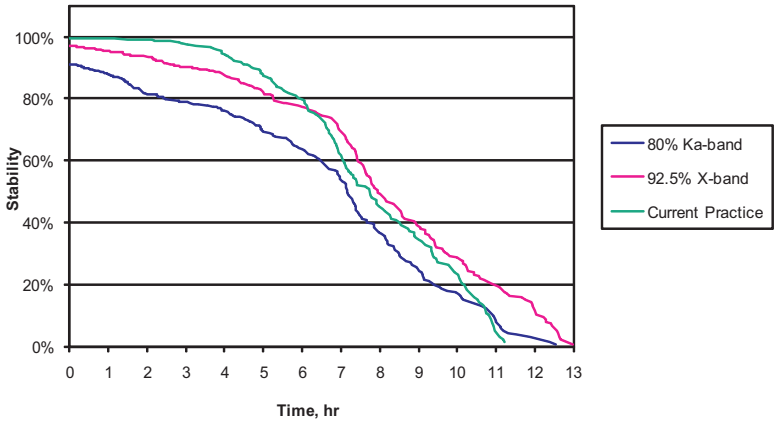

Figure 45. Stability vs. time, current practice, 90 percent MAR X-band and 80 percent MAR Ka-band, aggregate.

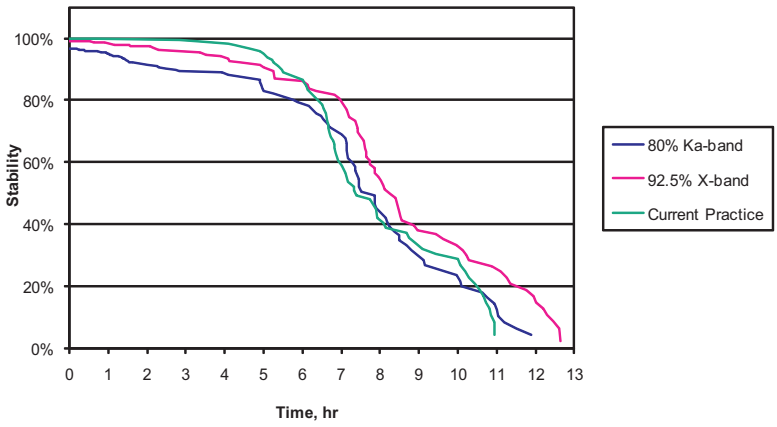

Figure 46. Stability vs. time, current practice, 90 percent MAR X-band and 80 percent MAR Ka-band, Goldstone.

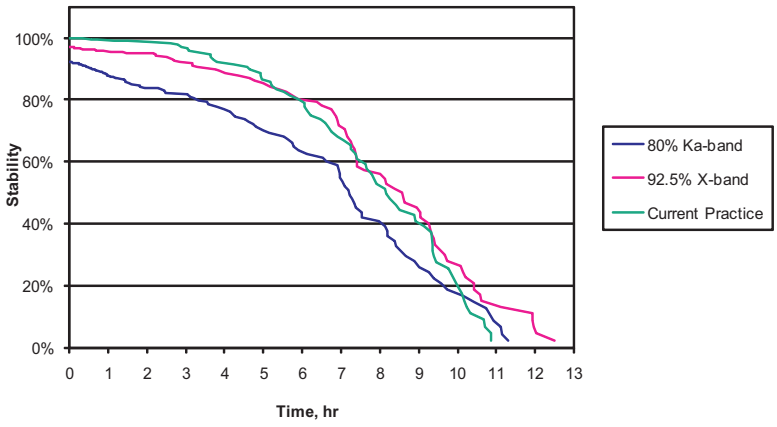

Figure 47. Stability vs. time, current practice, 90 percent MAR X-band and 80 percent MAR Ka-band, Canberra.

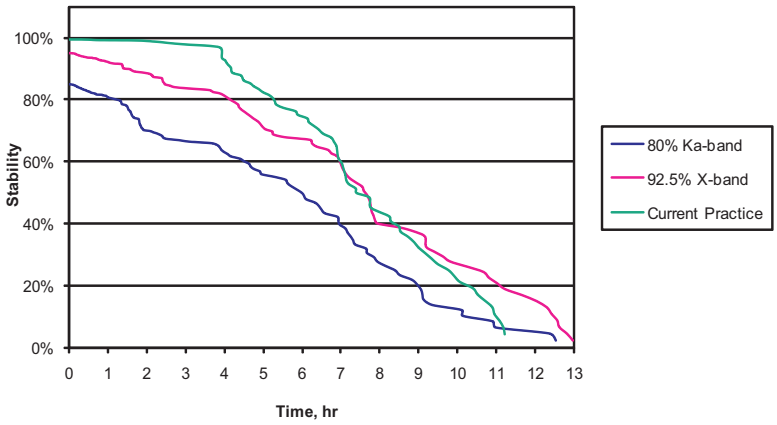

Figure 48. Stability vs. time, current practice, 90 percent MAR X-band and 80 percent MAR Ka-band, Madrid.

G. Delay-Throughput Performance

As mentioned before, the delay-throughput performance of the link was determined by using different loading factors (p_d) for a given MAR and then measuring the delay suffered by the data from its arrival into the spacecraft buffer until its successful transmission (i.e., the data were transmitted during a good period). The aggregate results of this exercise for the optimized Ka-band link and the optimized X-band link are shown in Figures 49 and 50.

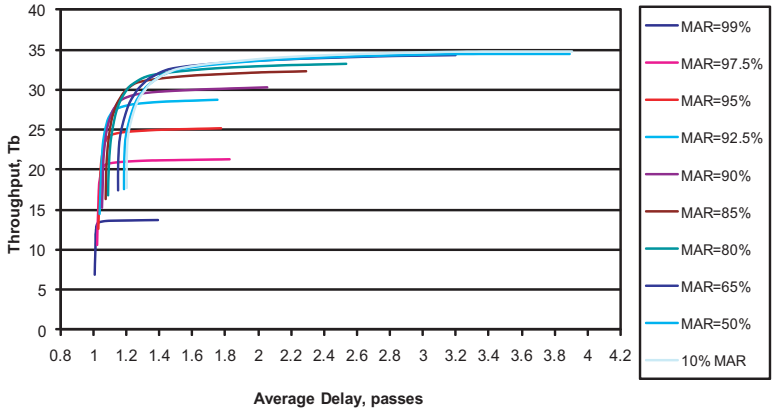

Figure 49. Ka-band delay-throughput curves for different MAR values, aggregate.

As seen from these curves, depending on the average delay requirements, different MAR values provide the maximum throughput; therefore, the aggregate delay-throughput performance of each link is defined by the upper envelope of the curves. By comparing

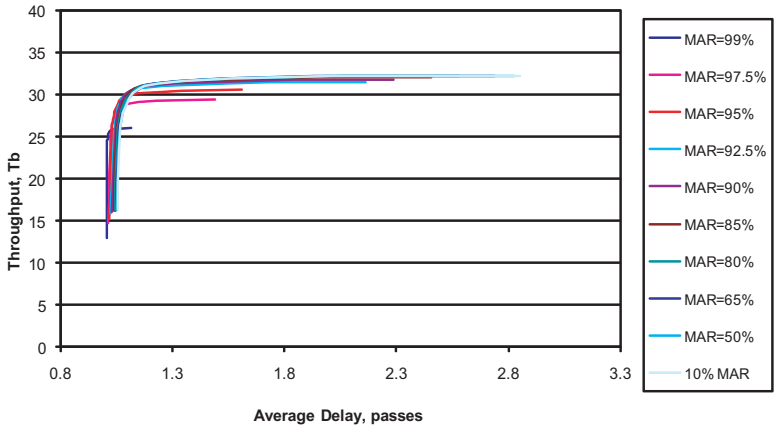

Figure 50. X-band delay-throughput curves for different MAR values, aggregate.

these upper envelopes, the delay-throughput performance of the optimized links could be compared with each other and with the delay-throughput performance of the current practice. These envelopes are shown in Figures 51 and 52. As seen from these figures, the Ka-band link will provide slightly higher throughput than the X-band system, provided that one is willing to accept longer delays in receiving the data. Similarly, both the optimized links provide significantly higher throughput (by more than 50 percent) than the current practice but, again, with longer delays.

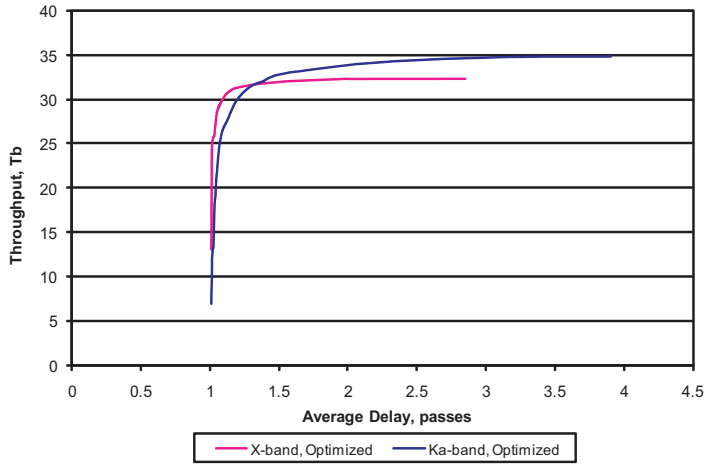

Figure 51. Optimized X-band and Optimized Ka-band delay-throughput envelopes, aggregate.

The Ka-band system consumes significantly less DC power than the X-band systems (80 W vs. 172 W). Therefore, the performance of the Ka-band system could be better compared to the X-band if the throughput is normalized by the DC power consumed. This

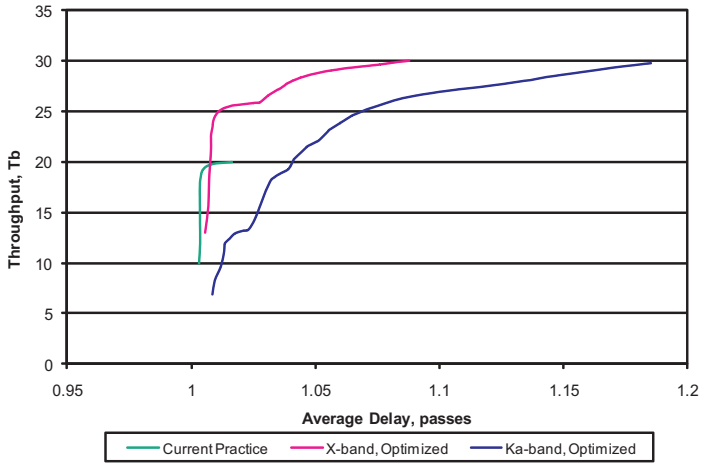

Figure 52. Comparison of the optimized X-band and optimized Ka-band delay-throughput performance to that of current practice, aggregate.

is shown in Figures 53 and 54. As seen from these figures, if longer delays are acceptable, the optimized Ka-band performs better than the optimized X-band link by approximately 3.7 dB and better than the current practice by approximately 5.7 dB. However, for very short delay requirements, the current practice provides the optimal solution. This result indicates that for bulk science data that can tolerate high latencies, Ka-band should be used, while for engineering and low-latency data the X-band link with a good margin should be used.

The analysis here is for the specific power amplifiers used for MRO. Depending on the amplifiers' efficiency, the Ka-band advantage could be greater or less than that depicted in Figures 53 and 54. As a rule of thumb, for the same frequency, the higher-powered amplifiers are more efficient than the lower-powered ones and amplifiers with the same output power are more efficient at lower frequencies than they are at higher frequencies. Therefore, if the X-band amplifier had the same 35-W RF output power as the Ka-band system, then the Ka-band advantage would be probably more than depicted in Figures 53 and 54. Similarly, if the Ka-band amplifier had the same 100 W RF output power as the X-band system, then the Ka-band advantage would be greater than that depicted in the figures. For the case where similar performance is expected out of both X-band and Ka-band, if the RF output for X-band is less than the 100 W analyzed here then the Ka-band RF power would be slightly less than 35 W, and therefore the Ka-band amplifier would be less efficient. In this case, the Ka-band advantage would be less than that depicted in the figures. Conversely, if the RF output for X-band is greater than 100 W, the Ka-band would also have to have a greater output power and therefore, a more efficient amplifier, In this case the Ka-band advantage would be greater than that obtained here. Finally, the Ka-band advantages depicted here could be significantly less if, instead of TWTAs, solid-state power amplifiers (SSPAs) are used. SSPAs are used for low-power applications and are substantially less efficient than TWTAs. Although the same general

rule of thumb applies to SSPAs regarding power output and frequency, the difference in efficiency between lower frequencies and higher frequencies could be substantially greater for SSPAs than for TWTAs.

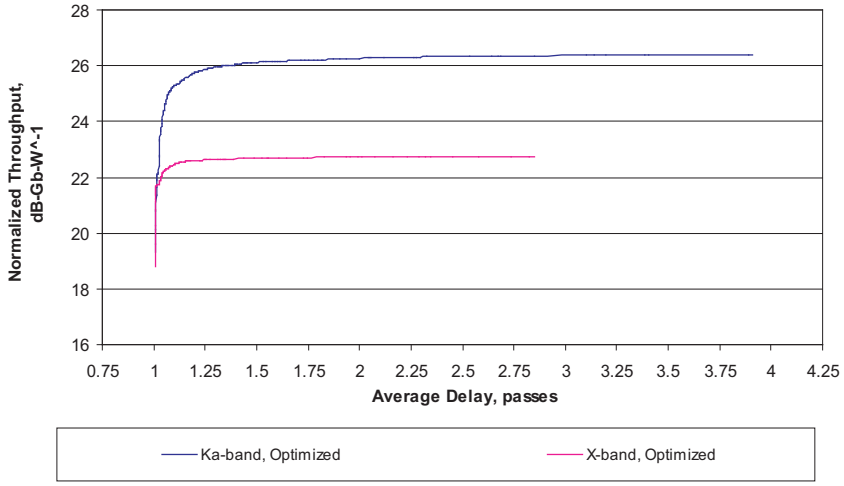

Figure 53. Optimized X-band and optimized Ka-band DC-power normalized delay-throughput envelopes, aggregate.

The delay-throughput analysis was also performed on a per-complex basis. For each case, the link was emulated only for passes over that complex and the delay-throughput performance was calculated. The normalized delay-throughput envelopes for each complex are shown in Figures 55 to 60.

Based on these figures, with the Ka-band link Goldstone and Canberra achieve 90 percent of their maximum throughput at relatively low average delay (1.05 passes and 1.26 passes respectively), while Madrid achieves 90 percent of the maximum throughput at a higher average delay (1.7 passes). This is probably due to the worse than expected weather that Madrid experienced over the period of emulation. Note that the aggregate performance achieves 90 percent of the maximum throughput at an average delay of 1.28 passes. This indicates that by using multiple sites, the effects of one site that suffers worse than average weather on the aggregate performance of the system is lessened.

Even though Ka-band systems are more power efficient in terms of bulk data throughput, at this time it is very unlikely that any deep-space mission in the near future will fly without an X-band system for emergency communications. Therefore, the Ka-band advantage depicted here may be further reduced once one considers this requirement. Having said this, because the X-band spectrum is much more limited than that for Ka-band, any mission requiring high data rates will probably use Ka-band.

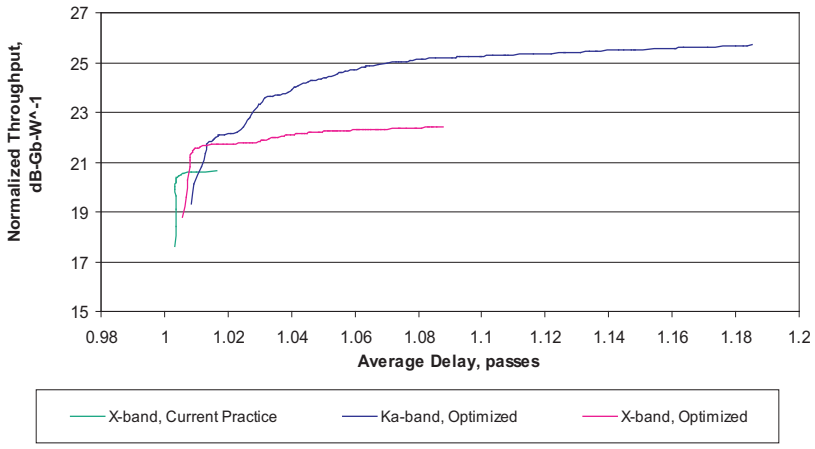

Figure 54. Comparison of the optimized X-band and optimized Ka-band DC-power normalized delay-throughput performance to that of current practice, aggregate.

H. Maximum of the Ratios of Amount of Data in Storage Before a Pass to the Amount of Data Collected Before that Pass (MRSC)

The plots of MRSC values vs. p_d for different MAR values and for the current practice are shown in Figures 61 to 68. For aggregate curves, as p_d increases, MRSC increases gradually at first then increases rapidly as p_d approaches 1 for all MARs. On a per-complex basis, however, the results are different. Goldstone and Canberra show only a gradual increase in MRSC as p_d increases but Madrid shows a very sharp increase as p_d approaches 1. This is to be expected. According to queueing theory, as the loading of the queueing system increases so does the size of the queue. This increase becomes more pronounced (approaching infinity) as the loading of the queue approaches its service rate (capacity). With Goldstone and Canberra, the actual capacity is near or better than expected. For Madrid, the actual capacity is less than expected. This means that for the same p_d value, Madrid is more heavily loaded relative to its actual capacity than either Goldstone or Canberra, hence the difference in the behavior of MRSC curves.

The MRSC values are generally larger for Ka-band than they are for X-band. This is to be expected because of the greater sensitivity of Ka-band to bad weather. For Madrid, this is most glaring because of the worse than expected weather at that complex.

Under the current practice, very little storage is required. This is to be expected since the current X-band link design provides a very reliable link, thus reducing the need for retransmissions and therefore, onboard storage.

For Ka-band, there is a significant drop in MRSC when the MAR is increased from 65 percent to 80 percent. Since there is very little difference in the link capacity for Ka-band between 10 percent MAR and 80 percent MAR, these figures indicate that by

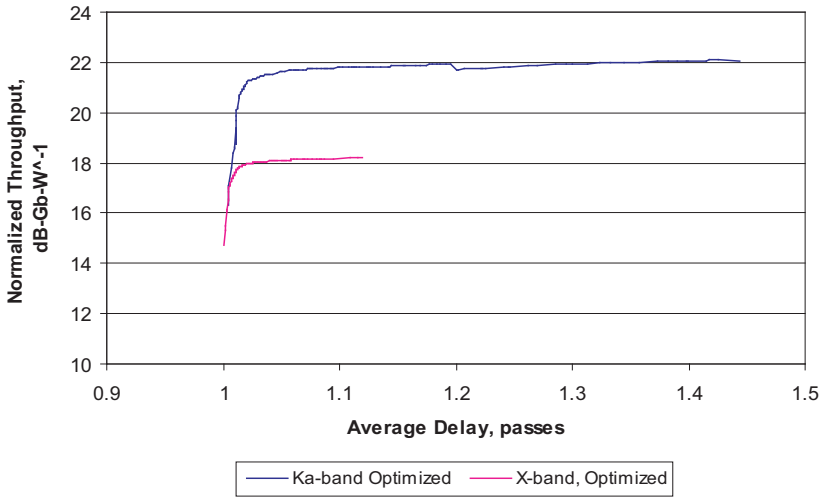

Figure 55. Optimized X-band and optimized Ka-band DC-power normalized delay-throughput envelopes, Goldstone.

designing the link for 80 percent MAR, the Ka-band storage requirements could be significantly reduced without a substantial loss of throughput. As Figure 61 indicates, for 80 percent MAR and $p_d = 0.95$, the MRSC is 3.28 for Ka-band. This means that with a storage greater than 3.3 times the maximum amount data collected before a pass, the Ka-band link could probably provide nearly 100 percent data completeness.

MRSC is not a perfect metric. It measures only the short-term variations of the amount of stored data on the spacecraft. Since the amount of data collected before a pass is dictated by the geometry and the duration of the pass as well the complex over which the pass takes place, MRSC values obtained through this emulation provide only a rough guideline for the storage requirements of the spacecraft. Further studies are needed to provide a more systematic method of determining Ka-band storage requirements.

IV. Conclusions

In this article, performance of the deep-space Ka-band link was compared to the X-band link through emulation, using WVR and AWVR sky brightness data, DSN performance parameters, MRO's geometry and DSN schedule, and MRO-like telecommunication capabilities models. The results indicate that the Ka-band link is significantly more power efficient than the X-band link provided that the Ka-band link is optimized for maximum expected capacity. Such a Ka-band link has a capacity of better than 3.5 dB over a similarly optimized X-band link and better than 5.5 dB over an X-band link designed according to current practices. Such a Ka-band link, however, will suffer significant outages. An analysis of outages indicates that these outages are not too long (on the average less than 30 min with a standard deviation of less than an hour) and large portions of the Ka-band tracking time are dominated by good weather.

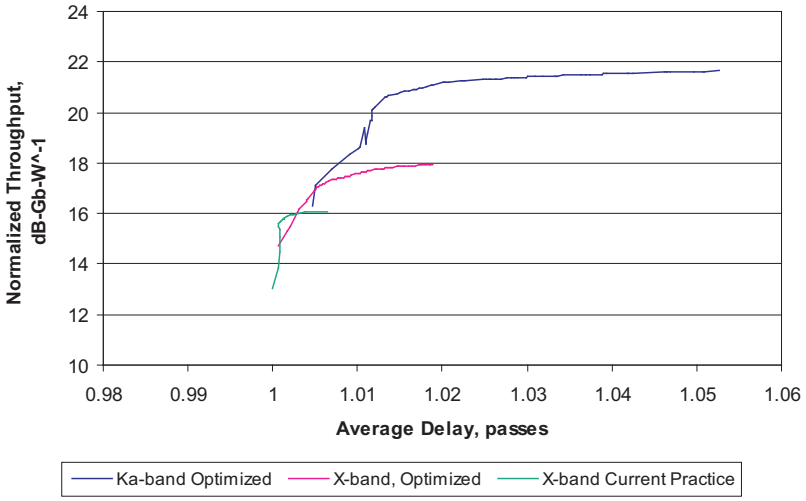

Figure 56. Comparison of the optimized X-band and optimized Ka-band DC-power normalized delay-throughput performance to that of current practice, Goldstone.

The results also indicate that the Ka-band link can be optimized subject to an 80 percent minimum availability requirement without a significant loss of capacity but with a significant reduction in data lost due to outages and a reasonable availability (better than 90 percent).

Retransmission schemes and additional spacecraft stroage are needed to assure data completeness. Our analysis indicates that by limiting the data collected before a pass to approximately 95 percent of the expected capacity of the pass, data completeness is virtually assured with a reasonably sized spacecraft storage (3 to 4 times the maximum amount of data collected before a pass) and with reasonable delay (less than 1.5 passes on the average). Our analysis, however, is not perfect and a more systematic approach is needed to confirm these results.

Our analysis indicates that Ka-band is not suitable for downlinking low-latency data because of its susceptibility to weather outages. For such data, it is recommended that X-band be used.

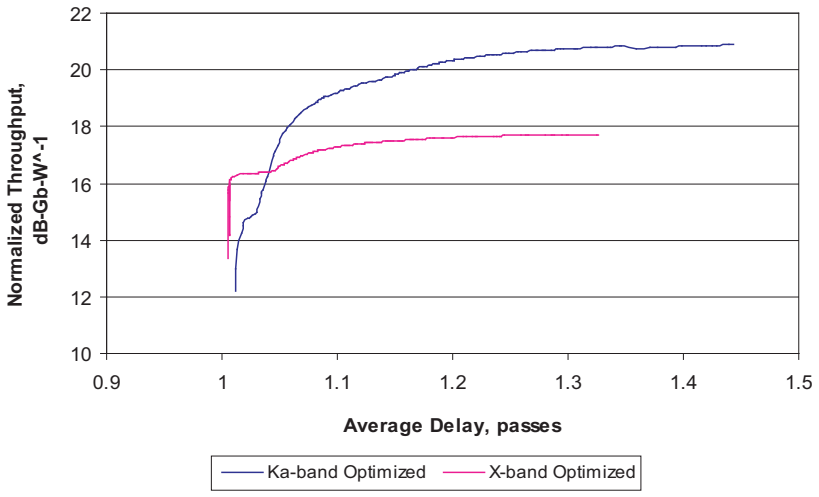

Figure 57. Optimized X-band and optimized Ka-band DC-power normalized delay-throughput envelopes, Canberra.

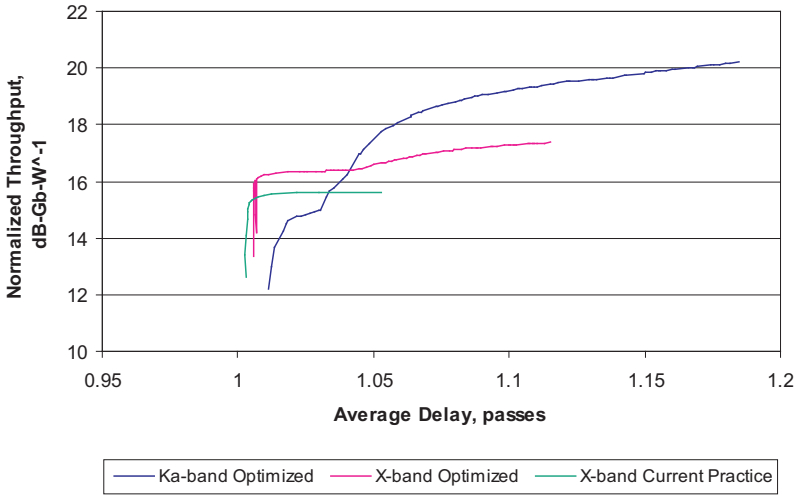

Figure 58. Comparison of the optimized X-band and optimized Ka-band DC-power normalized delay-throughput performance to that of current practice, Canberra.

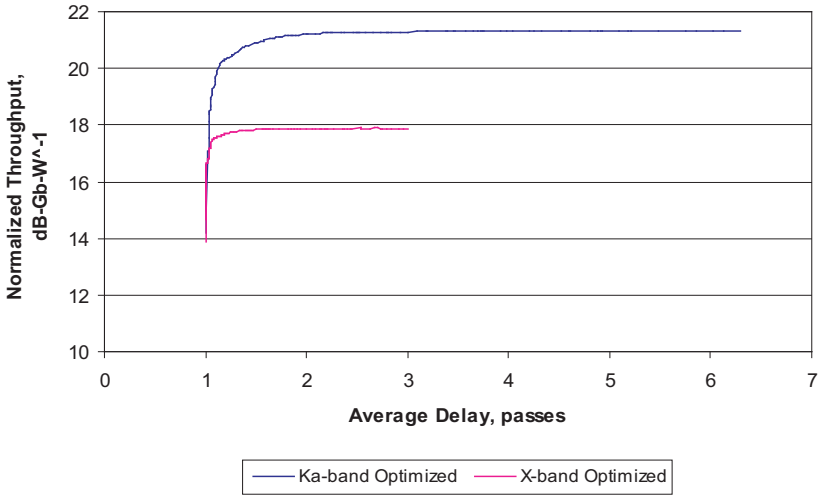

Figure 59. Optimized X-band and optimized Ka-band DC-power normalized delay-throughput envelopes, Madrid.

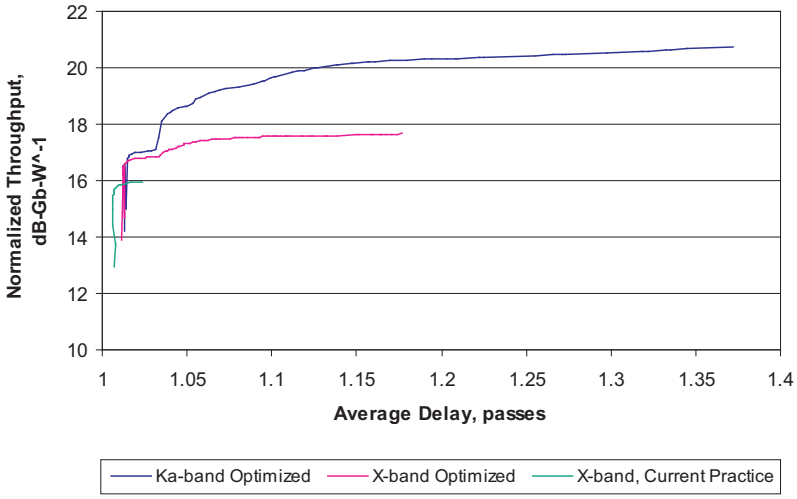

Figure 60. Comparison of the optimized X-band and optimized Ka-band DC-power normalized delay-throughput performance to that of current practice, Madrid.

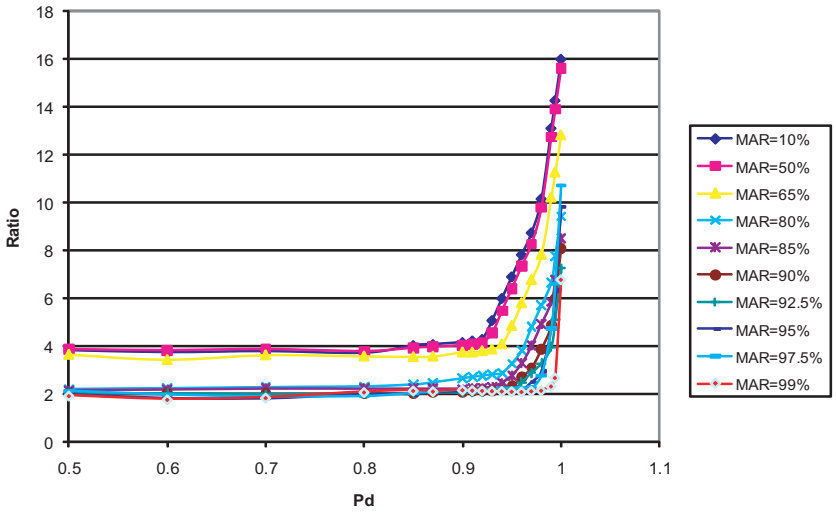

Figure 61. Ka-band MRSC vs. p_d for different MAR values, aggregate.

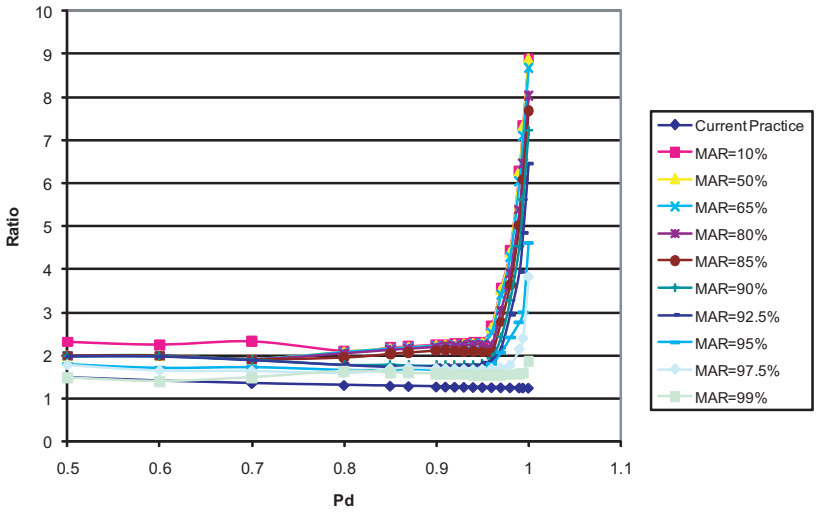

Figure 62. X-band MRSC vs. p_d for different MAR values and for current practice, aggregate.

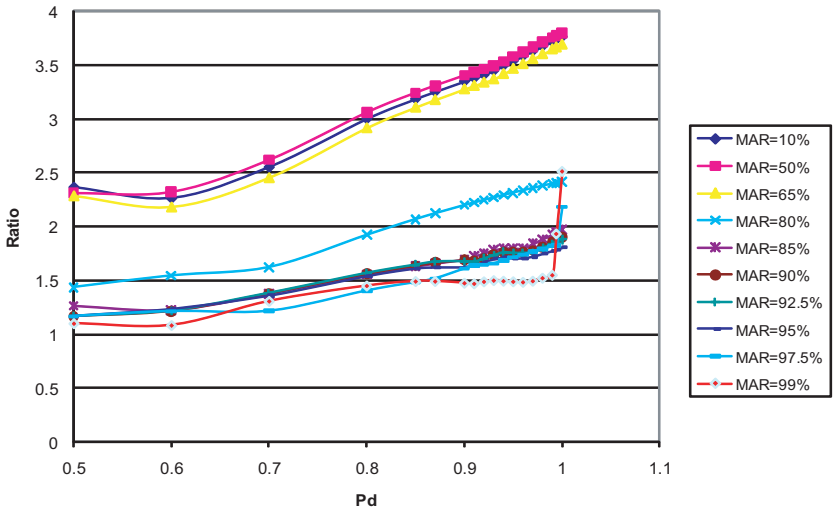

Figure 63. Ka-band MRSC vs. p_d for different MAR values, Goldstone.

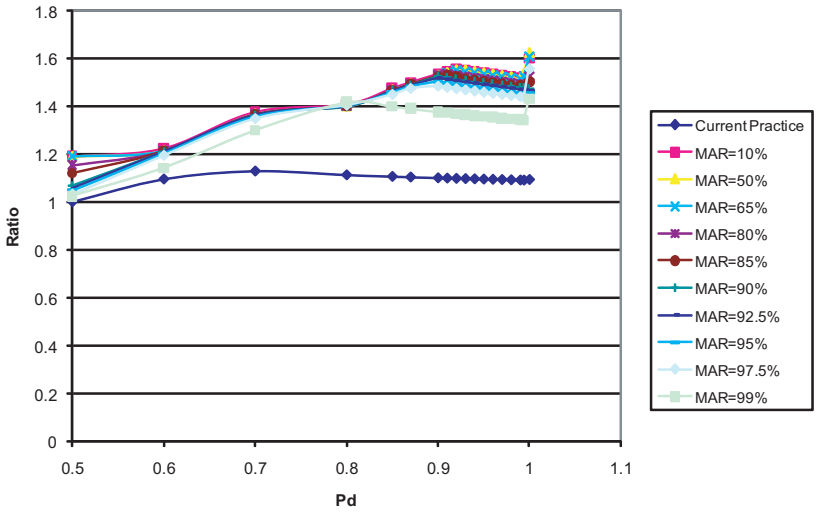

Figure 64. X-band MRSC vs. p_d for different MAR values and for current practice, Goldstone.

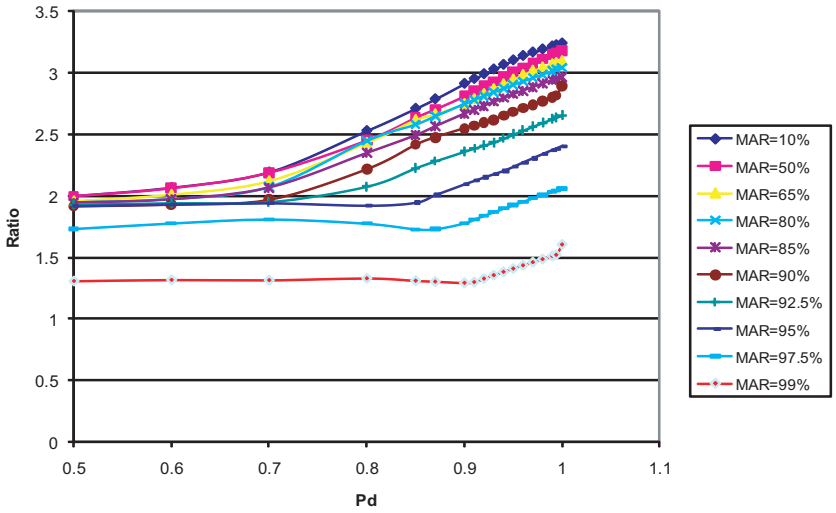

Figure 65. Ka-band MRSC vs. p_d for different MAR values, Canberra.

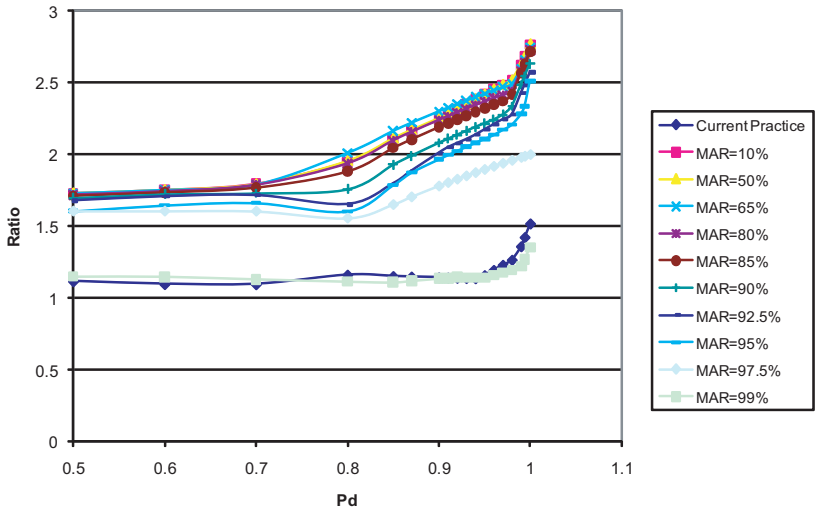

Figure 66. X-band MRSC vs. p_d for different MAR values and for current practice, Canberra.

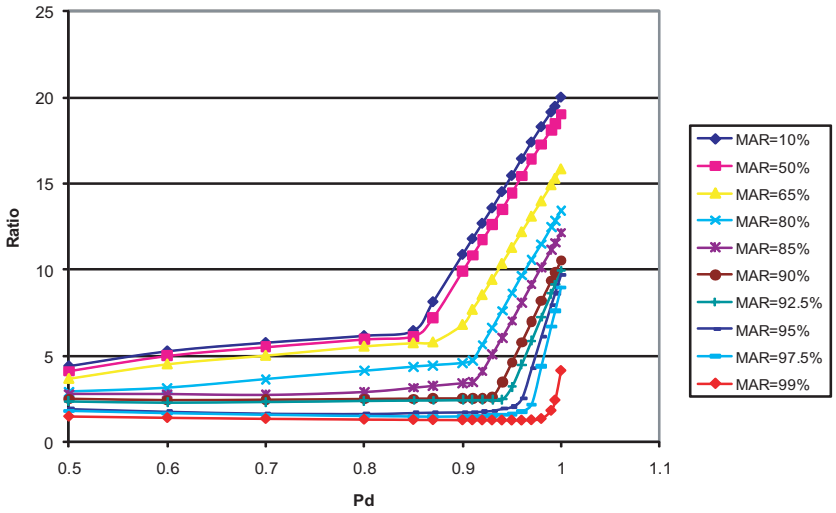

Figure 67. Ka-band MRSC vs. p_d for different MAR values, Madrid.

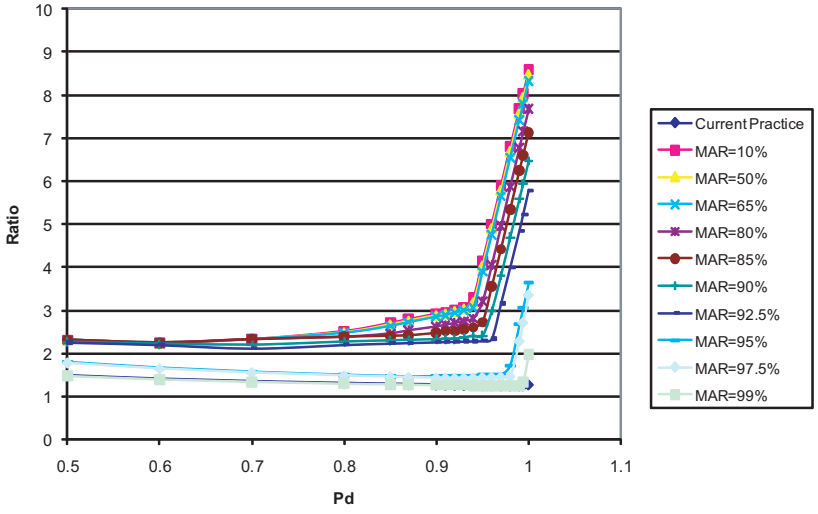

Figure 68. X-band MRSC vs. p_d for different MAR values and for current practice, Madrid.

References

[1] S. Shambayati, "Ka-band Telemetry Operations Concept: A Statistical Approach," *Proceedings of IEEE*, vol. 95, no. 11, pp. 2171-2179, Nov. 2007.

[2] S. Shambayati, "On Selecting the Size of a Spacecraft's Buffer," *The Interplanetary Network Progress Report*, vol. 42-174, Jet Propulsion Laboratory, Pasadena, California, pp. 1-25, August 15, 2008.

[3] S. Shambayati, J.S. Border, D.D. Morabito, and R. Mendoza, "MRO Ka-band Demonstration: Cruise Phase Lessons Learned," *IEEE Aerospace Conference 2007*, pp.1-17, Big Sky, Montana, March 4-10, 2007.

[4] R. W. Sniffin, Ed., *DSMS Telecommunications Link Design Handbook* DSN No. 810-005, Rev. E, Module 104, Rev. B: 34-m BWG Stations Telecommunications Interfaces, *http://deepspace.jpl.nasa.gov/dsndocs/810-005/104/104B.pdf*, Jet Propulsion Laboratory, Pasadena, California, August 1, 2005.

[5] S. Shambayati, F. Davarian, and D.D. Morabito, "Link Design and Planning for Mars Reconnaissance Orbiter (MRO) Ka-band (32 GHz) Telecom Demonstration," *IEEE Aerospace Conference*, Big Sky, Montana, March 5-12, 2005.

[6] S. Shambayati,"Weather Related Continuity and Completeness on Deep Space Ka-band Links: Statistics and Forecasting," *IEEE Aerospace Conference 2006*, pp.1-8,Big Sky, Montana, March 4-11, 2006.

[7] S. Shambayati, "Deep-Space Ka-band Link: Design, Continuity and Completeness," *IEEE Aerospace Conference*, Big Sky, Montana, March 1-8, 2008.